Universitetet i Stavanger

FACULTY OF SCIENCE AND TECHNOLOGY

MASTER'S THESIS

Study Programme/specialisation: Petroleum Engineering/Natural Gas	Spring semester, 2020 Open
Author: Hans Herrera Navarro	Hans Herrera Navarro Firmado digitalmente por Hans Herrera Navarro Fecha: 2020.07.15 09:01:29 +02'00' ..... (signature of author)
Supervisor(s): Prof. Zhixin Yu	
Title of the master's thesis: Influence of Indium on Cu/Zn and Cu/Zr catalysts for CO_2 hydrogenation to methanol	
Credits: 30 ECTS	
Keywords: CO_2 hydrogenation Methanol Indium Indium Oxide Cu-based catalysts Coprecipitation Wet Impregnation	Number of pages: 55 Stavanger, 15 July 2020

Acknowledgements

I would like to thank Kristian Stangeland, Huong Lan Huynh, and Prof. Zhixin Yu for all the support and patience while doing this research. It was exciting to work on this subject and I will always be thankful to all of you for accepting me as a part of the team.

Agradecido con mi familia y amigos por el apoyo moral, sobre todo en estos tiempos difíciles e inusuales. También agradezco mucho a Juana Ascencio, Erika Chong, Renata Brinceño y Rúbenson Barrios por prestarme la plata pa' venir a Noruega. Nadie presta toda esa plata así de chévere. Gente buena gente.

Sist men ikke minst, til Anje. Gleder meg til en fremtid sammen.

Abstract

The consequences of the anthropogenic carbon dioxide (CO_2) released into the atmosphere have been forecasted as devastating for the global environment. It is mandatory to take action now, and there are alternatives under development to mitigate and counteract the aftermath of climate change. One possible major contributor is carbon capture, utilization, and storage (CCUS), and several of its technologies have been successfully tested, such as the use of CO_2 as feedstock for different chemical processes. Converting emissions into methanol (CH_3OH) represents an interesting alternative for contributing to this solution. The conversion of CO_2 into valuable products is a technology with almost 100 years of history, although it has yet to reach optimal processing and maturity.

CO_2 hydrogenation to methanol is a process that requires moderate temperature and pressure to be effective. The catalysts used for converting CO_2 into methanol at a limited number of CO_2-to-methanol plants are based on a mix of metallic copper (Cu), zinc oxide (ZnO), and aluminum oxide (Al_2O_3). However, more efficient catalysts are necessary for large-scale implementation as the current catalyst is easily deactivated. Among many promoters tested to improve the catalyst's performance, zirconium oxide (ZrO_2) is considered an excellent promoter for Cu-based catalysts. Moreover, indium oxide (In_2O_3) has been investigated as a promising base catalyst due to its high methanol selectivity and good performance in high-temperature applications.

In this work, a set of Cu-based catalysts were synthesized using ZnO, ZrO_2, and In_2O_3 as promoters. The catalysts were prepared by coprecipitation or wet impregnation. Synthesized catalysts were characterized by N_2 physisorption, X-ray diffraction (XRD), N_2O titration, H_2-temperature programmed reduction, and inductively coupled plasma optical emission spectroscopy (ICP-OES).

The activity tests were performed in a packed bed reactor (PBR) at 230 ºC, 30 bars, and a feed stream of $H_2/CO_2/N_2$ with molar ratio 3:1:1. In_2O_3 improved the crystallite size of Copper particles and had a positive effect on the catalyst pore size, although has little impact in the catalytic activity of CO_2 hydrogenation to methanol. CuZr-based catalysts showed better performance in terms of methanol selectivity (ca. 52%) vs. CO_2 conversion (ca. 8%), however, CuZn catalysts are more active in terms of activity per area unit. Further investigations are required to achieve optimal ratios between Cu, Zn, Zr, and In_2O_3 for applications in industrial processes.

Table of Contents

List of Figures

List of Tables

1 Introduction

1.1 Background

Climate change and sustainable development are arguably the toughest and most explored research subjects in recent years due to their implication on the environment, society, technology, politics, and economy [1]. One of the ways to address climate change is carbon capture, utilization, and storage (CCUS), as anthropogenic CO_2 contributes significantly to greenhouse gas emissions [2]. Governments are imposing strict environmental laws and policies that limit emissions of various gases such as NO_x, CO_2, and SO_2, among which CO_2 is the most significant. Thus, CO_2 utilization processes are likely to play an important role in the future [3]. In a clean technology scenario, CO_2 utilization has been identified as a major contributor for cutting emissions within several sectors, as shown in Figure 1.1. Many alternative processes using CO_2 as feedstock are under development, which may become profitable in a low-carbon society [4].

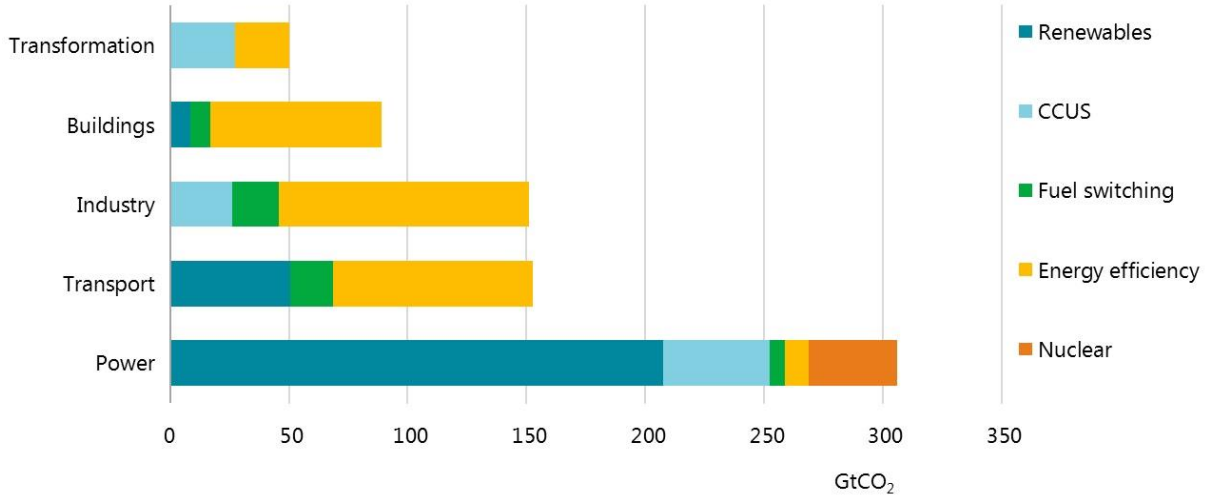

Figure 1.1. Global CO_2 emission reductions by technology and area sector, comparing Reference Technology Scenario to Clean Technology Scenario [5].

Methanol has been praised as an interesting alternative for moving away from fossil fuels towards cleaner energy solutions. In 2005, George A. Olah proposed that methanol rather than fossil fuels could be used as the primary energy carrier as well as feedstock for the synthesis of important hydrocarbons and their derivatives [6]. This model is based on "green" methanol produced from CO_2 and H_2 generated from renewable sources, creating a synthetic carbon-neutral cycle. One of the great advantages of the methanol economy compared to other

proposed future energy economies (e.g. hydrogen economy) is that methanol is highly versatile. Methanol is an important chemical feedstock used in a large array of chemical processes, such as methanol to olefins (MTO), paraffins (MTP), and gasoline (MTG). It can also be used as an alternative fuel in combustion engines or direct methanol fuel cells (DMFC) [7]. Furthermore, it can be utilized for wastewater treatment as it is readily biodegradable [8]. The given advantages and multiple uses of methanol and the current focus of reducing the CO_2 in the atmosphere are the main drivers for intensive CO_2-to-methanol technology investigations [9]. Figure 2.1 presents the projected total methanol demand by end-use for 2021.

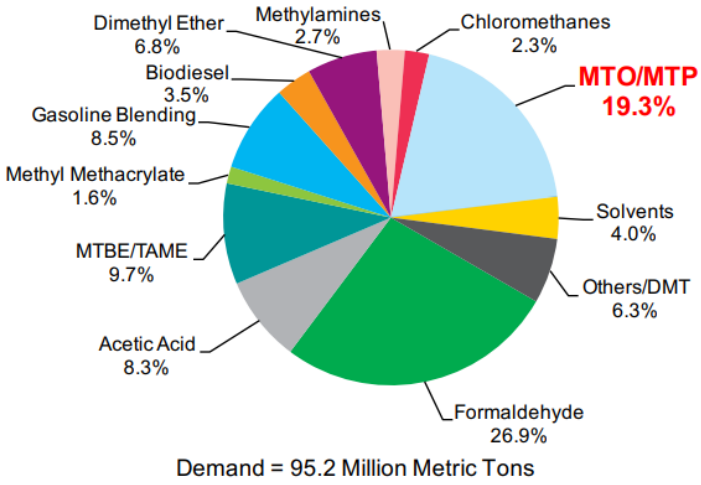

Figure 1.2. Total projected methanol demand by end-use for 2021 [10].

Currently, methanol is produced in a large-scale process from syngas, a mixture of CO, CO_2, and H_2, which is mostly generated from natural gas or coal [11]. The process for converting syngas and CO_2 to methanol is very similar. Thus, with the process and the infrastructure already in place, a transition into the CO_2-based methanol economy is feasible.

Syngas is converted to methanol over a heterogeneous catalyst composed of $Cu/ZnO/Al_2O_3$. Cu-based catalysts are also the most investigated system for CO_2 hydrogenation to methanol [12]. However, they are often prone to deactivation due to the more severe reaction environments in CO_2/H_2 mixtures [13]. To improve the activity and stability of Cu-based catalysts for CO_2 hydrogenation to methanol, different supports and promoters have been investigated (e.g. Ga_2O_3, Ce_2O_3, Cr_2O_3, TiO_2, ZrO_2, and In_2O_3) [14]. Typically, promoters increase the Cu dispersion thereby enhancing the catalyst's performance. Among other catalytic systems, In_2O_3-based catalysts have received considerable interest due to higher stability and methanol selectivity compared to Cu-based catalysts [15]. Typically, these

catalysts show stable performance with very high methanol selectivity over a wide temperature range but require higher reaction temperatures to obtain sufficient activity [16].

1.2 Scope of the work

There have been studies on indium oxide (In_2O_3) promotion of Cu-based catalysts. Sloczynski et al. [17] reported in 2006 that adding In_2O_3 to a $Cu/ZnO/ZrO_2$ catalyst considerably decreased the catalyst activity. More recent works are related to high selectivity and low conversion rates [18]. Other effects have been reported by Sadeghinia et al. [19] that adding In_2O_3 can lead to an increase in Cu surface area and oxygen vacancies but lower reaction rates. Further research is required in this field to achieve the optimal performance of In_2O_3 as a promoter in Cu/Zn and Cu/Zr catalysts.

The scope of this research is to gain insight into the effect of In_2O_3 on the catalytic performance of Cu/ZnO and Cu/ZrO_2 catalysts for methanol production. The focus is to determine the role of In_2O_3 on the catalytic activity and methanol selectivity. Well-ordered Cu/ZnO and Cu/ZrO_2 catalyst systems are synthesized by co-precipitation as a framework for In_2O_3 impregnation. Furthermore, a Cu/In_2O_3 catalyst is prepared for comparison. The catalysts are characterized by X-ray diffraction (XRD), transmission electron microscope (TEM), H_2-temperature-programmed reduction (TPR), N_2 adsorption-desorption, N_2O titration, and inductively coupled plasma optical emission spectroscopy (ICP-OES) to gain insight into the textural and physiochemical properties. The catalysts are tested for CO_2 hydrogenation to methanol at 230-270 °C and 30 bar.

2 Literature Review

2.1 Methanol: a brief history and industrial production

Methanol, or methyl alcohol, is a transparent liquid chemical compound soluble in water and quickly biodegradable. It is the simplest alcohol and has CH_3OH chemical formula. This compound has an ancient history, as it is documented that the Egyptians used methanol to preserve mummies [20]. The pre-industrialized period used methanol as wood spirit or wood vinegar [21]. After methanol was obtained by Robert Doyle in 1661 by simple distillation, Jean-Baptiste Dumas and Eugene Peligot determined the elemental composition in 1834. Not before 1905 research on methanol synthesis started when Paul Sabatier and Jean-Baptiste Senderens documented methanol decomposition using Cu-based catalysts [22].

Methanol production has been in constant growth since the methanol industry began in 1923 with the BASF plant in Germany using a ZnO/Cr_2O_3 catalyst. Natta [23] found that having Zn:Cr:Cu atomic ratios of 6:3:1 and 8:1:1 are quite active, but activity decreased considerably after a short period [24]. In 1963, Imperial Chemical Industries (ICI) started producing methanol at much lower pressures, by using a Cu/ZnO catalyst, the basis for the current methanol plants worldwide [25]. In 1971, an improved low-pressure methanol process was implemented with the Lurgi process, improving the overall reaction thermodynamics and efficiency [26]. During the new century, two major milestones have been accomplished. The first one is the George A. Olah Plant in Iceland that produces methanol from captured CO_2 since 2012 [27], and the second landmark is the opening of the largest methanol plant in the world: The Kaveh Plant in Iran with a reported production capacity of 2.3 million tonnes per annum. However, operations have been intermittent since its opening in 2017 [28]. In Europe, the largest methanol plant is in Norway, producing 2400 TPD (ca. 0.9 million tonnes per annum) and started operations in June 1997 [29].

2.2 Thermodynamics of CO_2 hydrogenation to methanol

CO_2 hydrogenation to methanol involves 3 main reactions: methanol synthesis reaction from CO_2 (Eq. 2.1), from CO (Eq. 2.2), and the reverse water-gas shift reaction (RWGS) as a side reaction (Eq. 3.3). From the reaction enthalpies, methanol synthesis is an exothermic process whereas the RWGS reaction is endothermic. Thus, according to Le Chatelier's principle, methanol production is favored at low temperatures and high pressures [30]. Thermodynamic

challenges start to appear as CO_2 is a very stable molecule, which requires sufficient energy to activate.

$$CO_2 + 3H_2 \leftrightarrow CH_3OH + H_2O \qquad \Delta H^0_{298} = -49.47\ KJ/mol \qquad (Eq.\ 2.1)$$

$$CO + 2H_2 \leftrightarrow CH_3OH \qquad \Delta H^0_{298} = -90.64\ KJ/mol \qquad (Eq.\ 2.2)$$

$$CO_2 + H_2 \leftrightarrow CO + H_2O \qquad \Delta H^0_{298} = +41.20\ KJ/mol \qquad (Eq.\ 2.3)$$

The effect of pressure and temperature on the thermodynamics of CO_2 hydrogenation to methanol is shown in Figure 2.1 (a) and (b) from two different studies. CO_2 is a very stable molecule, which requires sufficient energy to be activated, therefore, it is difficult to obtain enough reaction rates at very low temperatures. The drawback of operating at higher temperatures is that the RWGS reaction becomes more favorable, which results in lower methanol selectivity. Typically, methanol synthesis is conducted at 200-300 °C and 50-100 bar [31, 32]. The limitations of the thermodynamics are much stricter for CO_2 hydrogenation to methanol compared to methanol synthesis from syngas.

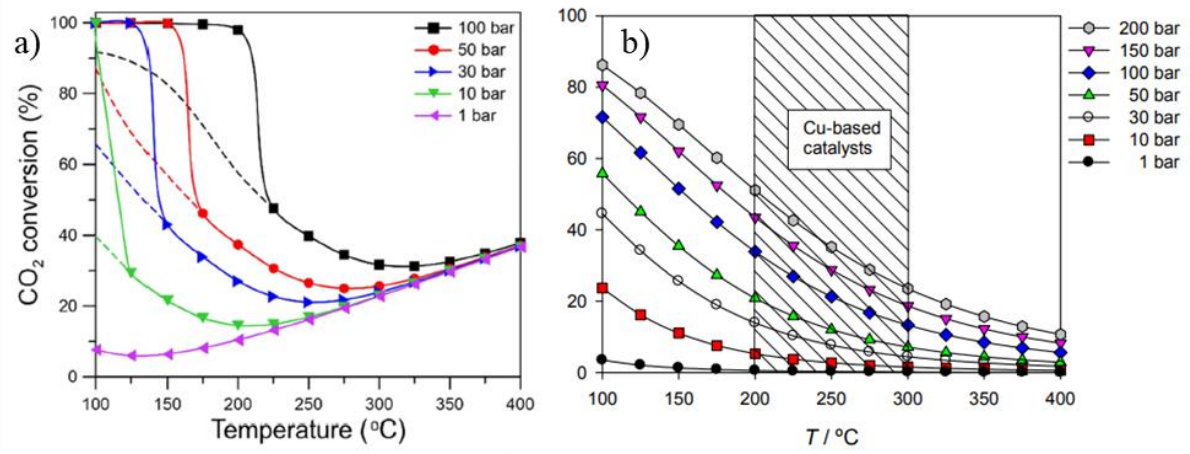

Figure 2.1. a) Effect of temperature and pressure on CO_2 conversion to methanol and CO (dashed lines represents gas-phase equilibrium) [30]. b) Effect of temperature and pressure on CO_2 conversion to methanol including the typical operating temperature range of industrial catalysts (dashed area) [32].

2.3 Catalysts for methanol synthesis from CO_2 hydrogenation

The Cu surface area plays a fundamental role in the overall activity for Cu/ZnO based catalysts. It is well known that Cu is the most active metal for methanol synthesis from CO_2 and H_2 [33]. However, metal oxides can have a significant influence on the activity and selectivity of Cu-based catalysts. Other systems include for example Pd/ZnO [34], which shows similar performance as Cu-based catalysts. In_2O_3-based catalyst has gained much interest lately as they

show very high methanol selectivity due to its limited activity for the RWGS reaction. The focus of this work is on the effect of In_2O_3 on Cu/ZnO and Cu/ZrO_2 for methanol synthesis, and therefore, this review will primarily cover these catalytic systems.

2.3.1 Copper - Zinc Oxide (Cu/ZnO) catalysts

Cu/ZnO-based catalysts, typically with Al_2O_3 as a structural promoter, is the most studied catalytic system for methanol synthesis. However, the role of ZnO in enhancing the catalyst's performance has been broadly debated. Studt et al. [35] noted that the presence or absence of ZnO can lead not only to changes in the activity but also in the reaction mechanism. Different promotional mechanisms have been proposed in the literature. Kakumoto [36] suggested that Zn sites are fundamental for the adsorption of the hydrogen ion (H^-). ZnO sites are also a possible site for the adsorption of the methoxy (CH_3O^-) intermediate, though as an alternative to Cu^+ sites since it has a higher formation barrier. Spencer [37] suggested that the synergy between Cu and ZnO depends on the operating conditions, but is due to hydrogen spillover from the ZnO to the metallic Cu on the surface. Natesakhawat et al. [38] proposed that the relationship between metallic Cu as the active site and the ZnO promoter was due to irregular morphology and defects induced by the addition of ZnO. Furthermore, ZnO also increases the Cu surface area, which is a common descriptor of the catalyst's activity. It has also been suggested that the role of the ZnO is related to the stabilization of the Cu^+ species on the surface [39].

In recent years, partial coverage of Cu by Zn or ZnO_x species is widely regarded as the active configuration in Cu/ZnO-based catalysts. Kattel et al. [33] obtained a volcano-type relationship between the activity and the fraction of Cu(111) covered by ZnO, as shown in Figure. 2.2. The trend depicted is similar to the results obtained by Fujitani et al. [40] for Zn-deposited on Cu(111). They found that the optimal turnover frequency (TOF) on Zn/Cu(111) catalyst was found at a Zn Coverage (ΘZn) of 0.19. Behrens et al. [41] proposed undistorted pure Cu(111) facets are not active and two aspects are required to dramatically increase the catalyst activity: available steps or irregularities in the Cu facets and the presence of Zn or ZnO_x at the defective Cu surface.

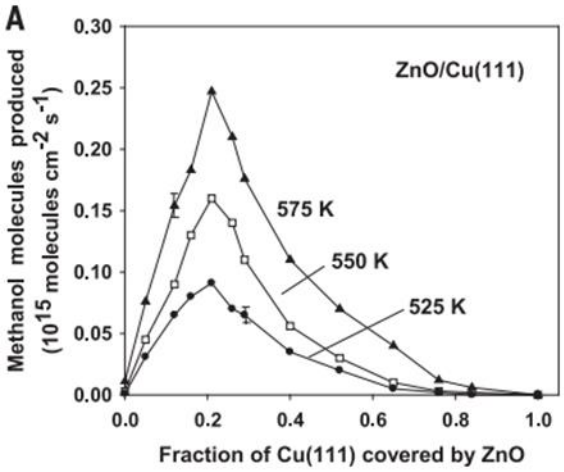

Figure 2.2. Rate of Conversion of CO_2 to methanol on Cu(111) vs. the fraction of the surface covered by Cu/ZrO_2 at three different reaction temperatures [33]. Observe the optimal range for methanol conversion slightly above 20%.

Complementing this observation, Karelovic and Ruiz [42] studied the Cu particle size on Cu/ZnO catalysts, since the Cu surface area is important for the activity of the catalyst. They showed that the methanol formation rate is independent of the particle size. However, they found a lower formation of CO and RWGS reactions over larger Cu particles. Van den Berg et al. [43] studied the structure sensitivity of Cu and CuZn catalysts, revealing a decrease in the turnover frequency (TOF) of the catalytic system when the Cu particle size is smaller than 8 nm. This was interpreted as methanol synthesis is favored when the Cu-based catalyst contains step-edge sites.

2.3.2 Zirconia (ZrO_2) as a promoter

The study of the synergy between Cu and ZrO_2 catalysts has been investigated thoroughly, especially in the last decade. More than 30 years ago, Gasser and Baiker [44] prepared Cu/ZrO_2 catalysts from Cu and Zr nitrates, as well as from Cu_7Zr_3, suggesting that the active sites of the catalysts have similar nature and activity. Kanoun et al. [45] were among the pioneers synthesizing Cu and Zr catalysts to produce methanol from CO_2, however, selectivities did not exceed 17%. Nitta et al. [46] reported much higher selectivities using Cu/Zr and Cu/Zr/Zn, though relatively low conversions. In both cases, Cu/ZrO_2 was found to enhance Cu dispersion. Schilke et al. [47] concluded that relatively small additions of ZrO_2 to Cu/SiO_2 favors the methanol conversion due to reactions occur on the active sites of both Cu and Zr. In later works, Zr has been identified to improve activity by controlling its phase [48]. Interactions between Cu, Zr, and doping Zn were analyzed by Arena et al. [49]. They concluded that the interaction

between Cu particles and both ZnO and ZrO_2 is beneficial for stabilizing the Cu active sites and enhance the adsorption/activation of H_2 and CO_2 for the reaction. In the early 2010s, tri-metal catalysts and precursors derived from hydrotalcite (HT) were the focus of many works, where Zr plays an important role in the dispersion of Cu, larger surface area and finally improving the methanol formation rate [38] [25-27].

The effect of different ZrO_2 phases on Cu-based catalysts is still under discussion. Several works have come to differing conclusions in regards to which is the most active ZrO_2 phase as well as the optimal preparation method for achieving the appropriate phase and high Cu dispersion. Samson et al. [50] found a direct relationship between the morphology of the ZrO_2 phase and the catalyst activity. Despite being the most thermodynamically unstable phase, Cu supported on tetragonal ZrO_2 (t-ZrO_2) was found as the most active catalyst, attributed to a higher concentration of acidic centers formed with the participation of Cu cations connected to the oxygen vacancies.

Witoon et al. [51] investigated the activity of Cu supported on different ZrO_2 phases: amorphous (a-ZrO_2), monoclinic (m-ZrO_2), and t-ZrO_2. The highest activity was obtained over Cu/a-ZrO_2, which also had the highest Cu surface area. However, the methanol TOF over the t- phase was between 1.1–1.5 and 1.6–3.6 times higher than Cu/a-ZrO_2 and Cu/m-ZrO_2, respectively. The relationship between the ZrO_2 phase and the CO_2 conversion and methanol selectivity is shown in Figure 2.3.

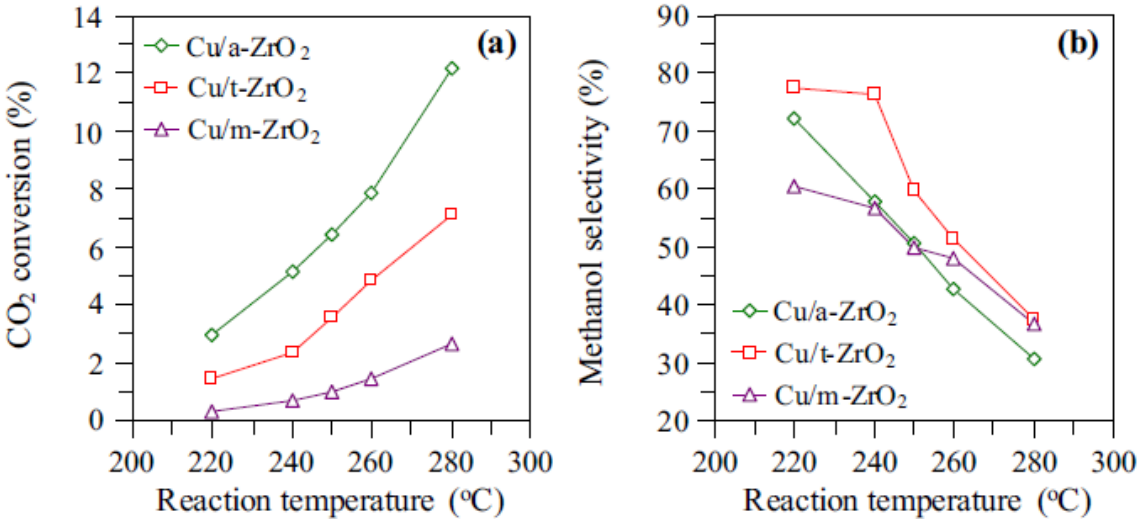

Figure 2.3. CO_2 conversion (a) and methanol selectivity (b) as a function of the reaction temperature on a-ZrO_2, t-ZrO_2 , and m-ZrO_2 [51].

Tada et al. [52] also found that a-ZrO_2 resulted in higher conversions compared to m-ZrO_2 and t-ZrO_2, which was attributed to higher Cu dispersion. In addition, weaker methanol adsorption was measured on a-ZrO_2 species, leading to higher methanol selectivity by limiting methanol decomposition. Ro et al. [53] found that the formation of Cu-ZrO_2 interfacial sites increased the TOF to methanol, indicating that the number of interfacial sites significantly influences the activity of Cu-ZrO_2 catalysts. Wang et al. [54] and Larmier et al. [55] also concluded that larger Cu surface areas do not necessarily mean a higher activity of Cu-ZrO_2 based catalysts. More recently, Fujiwara et al. [56] studied the influence of the particle size with highly loaded CuO on ZrO_2 catalysts synthesized via spray pyrolysis. They observed that when the catalysts are prepared at a slower rate, it is more likely to result in smaller ZrO_2 particles, which increases the number of interfacial sites and show higher activity.

Li and Chen [57] summarized the current status of research on Cu-Zr interaction and proposed further investigations on the effect of each phase on the catalytic performance. Their findings are shown in Figure 2.4. In general, Cu/ZrO_2 systems present four typical surface properties, i.e., acidic, basic, oxidizing, and reducing, although relatively weak. However, the structure sensitivity plays an important role in promoting the CuZr system for methanol synthesis. The authors also propose further research in the oxide-oxide interactions (e.g. ZnO-ZrO_2 interface).

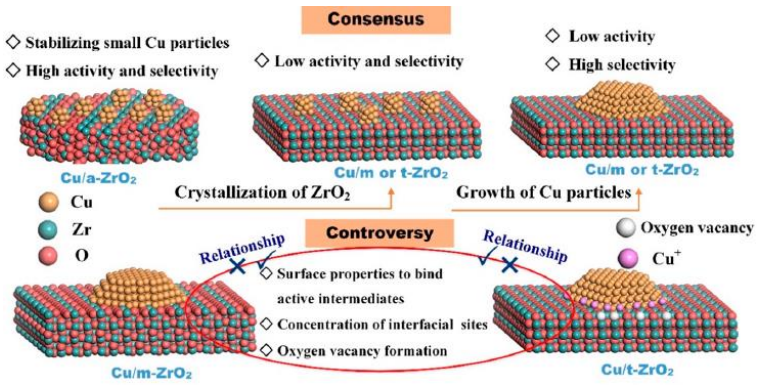

Figure 2.4. Effects of Zr phases on the catalytic performance of Cu/ZrO_2 catalysts, according to [57].

Several studies have also investigated the effect of promoters on Cu-ZrO_2 catalysts. Tada et al. [58] considered the addition of Ag into Cu-ZrO_2, evaluated the quality of the active sites by changing space velocities, and concluded an improvement in the methanol selectivity compared to a Cu-ZrO_2 catalytic system. The formation of an Ag-Cu alloy resulted in a new active species for the CO_2 hydrogenation process.

Hengne et al. [59] prepared ZrO_2 supported Ni-Sn catalysts and studied the effect of adding In_2O_3 as a promoter. They showed that a 99% selectivity was achieved, together with high

conversion rates and good stability. There are many other works including vanadium oxide [45], In_2O_3 [19], TiO_2 [47], Y_2O_3, La_2O_3, Ce_2O_3, and Al_2O_3 [60, 61], although the latter two are for methanol steam reforming and methanol fuel cells processes.

2.3.3 In_2O_3 catalysts for CO_2 hydrogenation to methanol

In_2O_3 alone can also be used as a catalyst for the CO_2 conversion to methanol. For instance, In_2O_3 catalysts have shown interesting results in terms of activity and selectivity, in some cases reporting selectivity values close to 100% when ZrO_2 promoter is present [62]. Studies conclude that high selectivity was achieved due to In_2O_3 not being particularly active for the RWGS reaction [16], even at a broad range of temperatures of 450 – 673 K [63]. Another important effect from ZrO_2 over In_2O_3 is the suppression of dissociative CO_2 and stabilization of intermediates on the catalyst surface [64].

Ye et al. [15] proposed a reaction mechanism over In_2O_3(110) catalyst using density functional theory (DFT) calculations, favoring the HCOO route. More recently, Frei et al. [65] carried out a similar study over In_2O_3(111), concluding that the activation energy (Ea) determined for the CO_2 to methanol synthesis was higher than the one for the RWGS reaction, explaining the superior methanol selectivity of the catalyst. In the last few years, Chen et al. [66], Chou and Lobo [67], and Frei et al. [68] have studied the promotional effect of ZrO_2 on In_2O_3, which resulted in high methanol selectivity and increased the number of active sites.

2.3.4 In_2O_3 as promoter for CO_2 hydrogenation to methanol

Ever since the study carried out by Sloczynski et al. [17] and its discouraging results in terms of CO_2 conversion, In_2O_3 has received little attention as an effective promoter over Cu-based catalysts. However, the advantages of new analyses and tools to elucidate reaction mechanisms in the CO_2 hydrogenation reaction have encouraged scientists to test materials once discarded in the past. For instance, Yao et al. [18] and Chamssine [69] studied the effects of In_2O_3 on CuZr and hydrotalcite-like catalysts respectively, by varying both the Cu load and the In_2O_3 promoting load, and demonstrated good methanol selectivity between 50% and 75%, as well as reaction stability for long-run reactions.

The latest works by Sadeghinia et al. [19] and Gao et al. [70] reveal the promotional effects to the structural properties of adding In_2O_3 to Cu-based and CuZr catalysts in terms of larger surface area and pore size distribution, but mixed results in terms of CO_2 conversion and

methanol selectivity. The limited investigations and the lack of a solid consensus on catalytic activity for CO_2 hydrogenation to methanol are yet other drivers for carrying out investigations on the promotional effects of indium over Cu-based catalytic systems.

2.4 Reaction Mechanisms for CO_2 Hydrogenation to Methanol

2.4.1 Cu/ZnO catalysts

Several studies have focused on the reaction mechanism of CO_2 hydrogenation to methanol over Cu-based catalysts. Formate (HCOO) and methoxy (H_3CO) intermediates are the most common species identified for methanol synthesis [71] and were also observed in *In Situ Fourier Transform - Infra-Red* (FT-IR) studies [72]. In literature, the reaction pathway that is most often reported goes through the formate intermediate and can be simplified to 7 elementary steps (Eqs. 2.4 to 2.10), where * denotes the active sites.

$$CO_2^* + H^* \rightleftarrows HCOO^* + * \qquad (Eq.2.4)$$

$$HCOO^* + H^* \rightleftarrows H_2COO^* + * \qquad (Eq.2.5)$$

$$H_2COO^* + H^* \rightleftarrows H_2COOH^* \qquad (Eq.2.6)$$

$$H_2COOH^* \rightleftarrows H_2CO^* + OH^* \qquad (Eq.2.7)$$

$$H_2CO^* + H^* \rightleftarrows H_3CO^* + * \qquad (Eq.2.8)$$

$$H_3CO^* + H^* \rightleftarrows CH_3OH^* + * \qquad (Eq.2.9)$$

$$CH_3OH^* \rightleftarrows CH_3OH^{(g)} + * \qquad (Eq.2.10)$$

Grabow and Mavrikakis [73] presented a comprehensive study of the reaction mechanism, which is based on energetics over Cu(111) from DFT corrected by experimental values. Figure 2.5 illustrates several intermediates and their binding configuration on Cu(111). In the figure, red dots represent oxygen, black dots show carbon, and blues denote hydrogen. Hydroxy (OH) and carbon monoxide (CO) molecules are not shown for simplicity. The Cu surface is represented by the brown dots. They found that the main route for CO_2 hydrogenation to methanol was through HCOO* → HCOOH* → H_2COOH* → H_2CO* → H_3CO* → H_3COH*. CO could also be hydrogenated to methanol but follow a different pathway (CO → HCO → H_2CO → H_3CO → H_3COH).

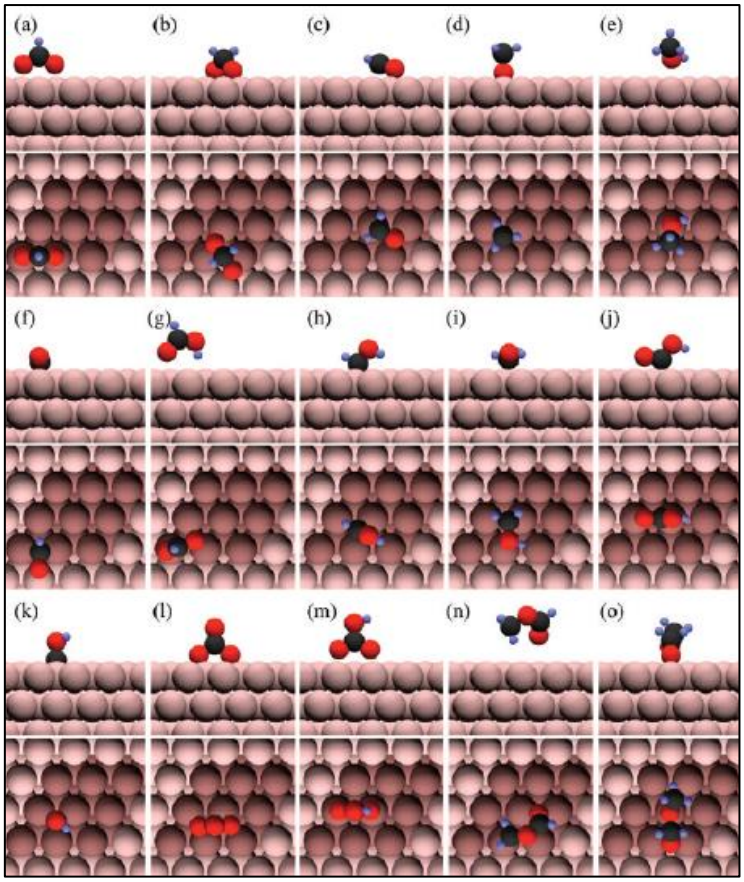

Figure 2.5. Adsorption states of selected intermediates for CO_2 to methanol reaction on Cu(111). Top row: (a) formate, (b) dioxymethylene, (c) formaldehyde, (d) methoxy, (e) methanol. Middle row: (f) formyl, (g) formic acid, (h) hydroxymethylene, (i) hydroxymethyl, (j) carboxyl. Bottom row: (k) hydroxymethylidyne, (l) carbonate, (m) bicarbonate, (n) methyl formate, (o) methoxyoxymethylene. [73].

Behrens et al. [41] conducted DFT calculations to investigate the role of Zn on Cu. Methanol synthesis through the formate pathway was compared over Cu(111), Cu(211), and CuZn(211). They found that Cu steps in Cu(211) lowered the barriers and increased the stability of reaction intermediates, which was further enhanced by Zn addition to Cu(211).

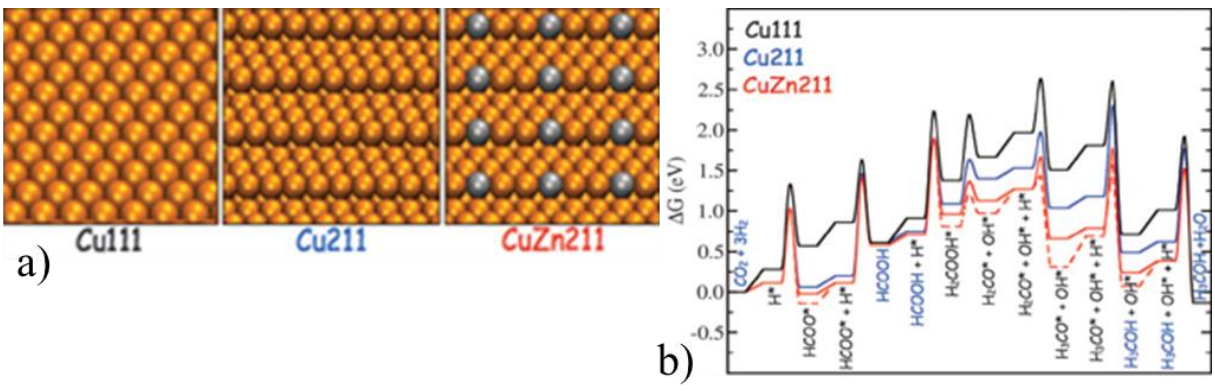

Figure 2.6. a) Graphic representation of Cu and CuZn arrangements containing both Cu (yellow spheres) and zinc (silver). b) Gibbs free-energy diagram (ΔG) for CO_2 to methanol reaction from DFT calculations [41].

Other routes from CO_2 to methanol have also been explored. Zhao el at. [74] studied the reaction network on Cu(111) using density functional theory (DFT) calculations. They found that methanol synthesis through the formate intermediate was unlikely due to high barriers. A hydrogen transfer mechanism was observed in the presence of co-adsorbed H_2O that made the carboxyl (COOH) route more favorable. The subsequent steps were through the formation of COHOH, followed by COH, HCOH, and finally methanol (CH_3OH).

2.4.2 Cu/ZrO_2 catalysts

Wang et al. [54] and Larmier et al. [55] proposed a similar reaction mechanism over Cu/ZrO_2 catalysts. Both studies conclude that hydrogenation of formate is the rate-limiting step in the hydrogenation process. They also pointed out the crucial role of the molecular interaction between the Cu and Zr compared to other structural properties, such as surface area or oxygen vacancies. Figure 2.7 shows the reaction mechanism determined by Larmier et al., which is the same as the reaction route typically proposed over Cu and Cu/ZnO systems.

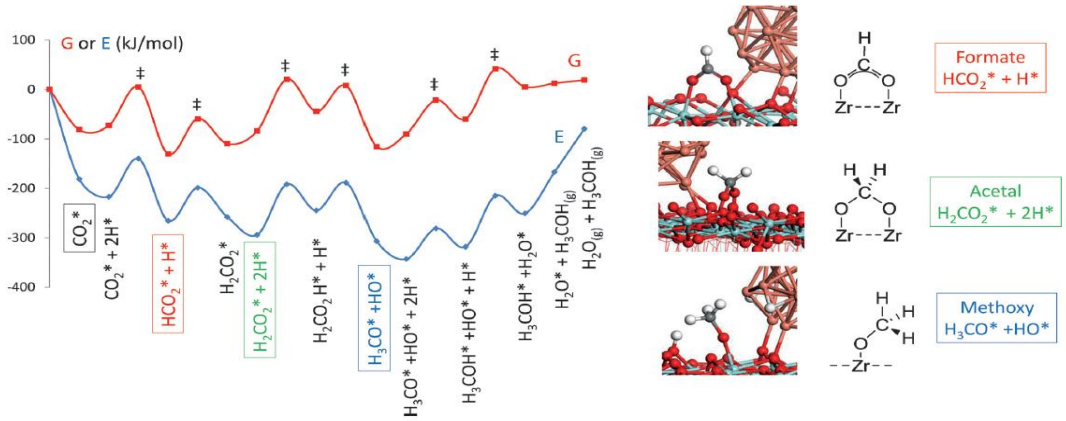

Figure 2.7. Reaction Mechanism, Energy, and Gibbs Free Energy (ΔG) for the CO_2 hydrogenation to methanol at Cu/ZrO_2 interface [55].

2.4.3 In_2O_3 catalysts

Ye et al. [15] and Frei et al. [65] studied the reaction mechanism of CO_2 hydrogenation to methanol using DFT calculations over In_2O_3(110) and In_2O_3(111) catalysts, respectively. A common simplified route proceeds as $CO_2 + H_2$ (adsorbed) → HCOO* → HCOOH* → CH_2O* → CH_3O* → CH_3OH*, which is similar to Cu-based catalysts. The binding energy of intermediates is different on In_2O_3 compared to Cu and the proposed rate-limiting step depends on the In_2O_3 lattice. Figure 2.8 shows a representation of the In_2O_3(111) lattice and the adsorption of CO_2 and H_2.

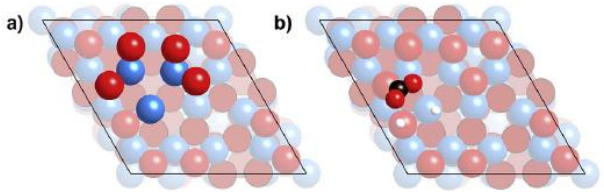

Figure 2.8. (a) Top-view of the In_2O_{3-x}(111) surface, with an oxygen vacancy per (1x1) cell. (b) Top view of the activated co-adsorption of CO_2 and H_2 on In_2O_{3-x}(111). Color code: In (blue), O (red), C (black), and H (white) [65].

Figure 2.9 depicts the structures of the adsorbed reaction intermediates. It represents the mechanistic route for the reaction, from left to right and top to bottom. Color code: H (white), O (red), C (black) and In (grey).

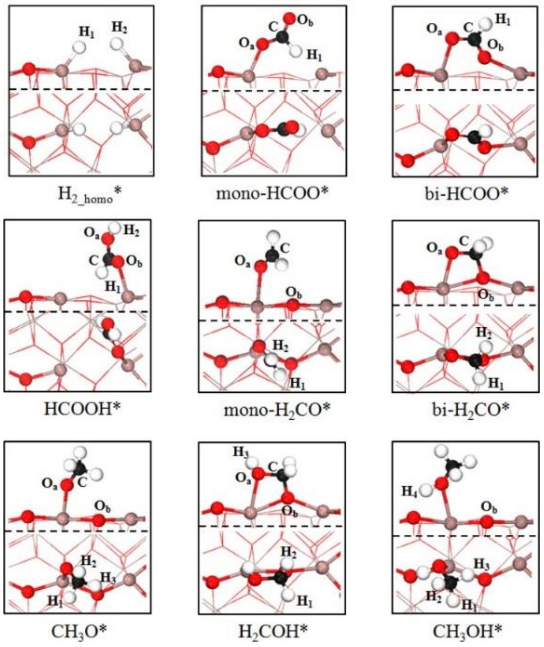

Figure 2.9. Optimized adsorption structures of the reaction intermediates involved in CO_2 hydrogenation to methanol on defective In_2O_3(110) surface [15].

2.5 Catalyst Synthesis

There are numerous catalyst preparation methods and every catalyst can be synthesized using different techniques. However, there are three basic steps that synthesis of supported metal oxides (SMOs) have in common: preparation of precursor, precursor processing (e.g., via calcination or pyrolysis), and activation of the precursor to obtaining the final active catalyst [75]. Herein, only the theoretical basis of the synthesis methods used in this work will be presented.

2.5.1 Coprecipitation

Synthesis by coprecipitation is a method where a solid is precipitated from a solution that contains precursors of both the support and the active metal oxides. It is initiated by mixing the solution with a precipitating agent, which has two possible effects. First, condensation of the precursor by changing the solution pH and second, introduces ions to the solution to exceed the solubility of the product. After precipitation, aging steps can be carried out for crystal growth. Lastly, filtering and washing the counterions results in the final precursor [76]. The advantages of this procedure are a better spatially distributed framework of the oxide materials compared to other methods, which will allow better interaction between the support and the active species, also with reduced exposure of the active species to the catalytic surface as a downside. For the latter reason, it is often to find density calculation results overestimating actual values [76].

Several parameters will influence the structure of the precursors synthesized by coprecipitation: precipitating agent, pH control, efficient mixing, washing, aging, and filtering. Supporting the influence of the preparation parameters in the preparation of catalysts, Figure 2.10 describes the variation of the surface area with the pH during the coprecipitation method, from three different ZrO_2 catalysts [77].

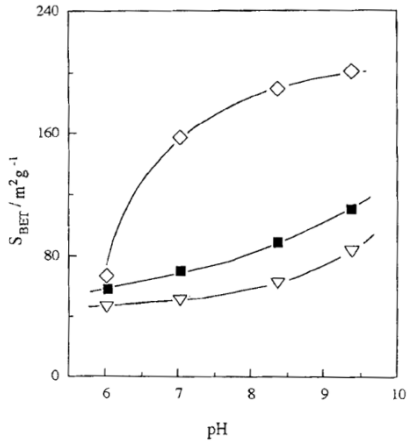

Figure 2.10. Correlation of surface area vs. pH change in preparation by precipitation. Precursors are labeled as (□) ZrO2▪ H_2O, ZrO_2 (Δ) and SO_4^-/ZrO_2 (■) [77]

2.5.2 Wet impregnation

This relatively simple procedure consists of contacting a solid (solute) with a solution containing the materials to be deposited on the surface (support). During impregnation, there

are two major phenomena for the synthesis process: a *diffusion* process, where the solute spreads into the pores of the support and the *adsorption* process, where the solute attaches into the pores [78].

After a homogeneous solution is achieved with vigorous stirring for a long period, samples are dried to remove the solvent solution. This process is also common with the coprecipitation method. After the drying process, the precursor is ready for calcination.

2.5.3 Calcination

Calcination is a procedure where the as-prepared catalyst is heated to a high temperature, usually higher than the desired reaction temperature, in order to decompose the metal precursor by forming oxide and to remove impurities (water, CO_2, etc). High calcination temperatures can lead to a crystallization of the support and a loss of surface area [76]. When dealing with bimetallic catalysts, rigorous control of calcination temperature is required to avoid the formation of two separate oxides or the segregation of one of the components [79].

2.5.4 Reduction

The reduction process often occurs right before the catalyst is tested for the desired reaction, hence, it is mostly performed in the reactor. It consists of treating the catalyst with diluted hydrogen in an inert gas (usually N_2, He or Ar) at high temperatures, aiming to transform the oxide into an active metallic compound. Hydrogen is diluted to limit the rise of the adiabatic temperature, preventing particle *sintering*. To investigate and evaluate the reducibility of the catalyst, a temperature-programmed reduction (TPR) analysis is performed [80].

2.6 Catalyst Characterization

This section will present the different techniques, procedures, and theoretical background for the characterization of physio-chemical properties and morphology of the catalysts.

2.6.1 X-Ray Diffraction (XRD)

The powder X-ray diffraction technique allows evaluating the nature, concentration, and distribution of the crystals present in the catalyst, among other characteristics. XRD considers transverse planes of atoms periodically spaced, which is hit by upcoming waves (X-rays) at a specific angle. To generate interference patterns that can be interpreted, the wavelength (λ) has

to be in the same order of magnitude as the interatomic space or distance (*d*), which is the case for the X-Rays (λ ≈ 1 Årmstrong). The ratio between λ and *d* is given by Bragg's Law (Eq. 2.11) [81].

$$n\lambda = 2d * sin\,\theta \qquad (Eq.\ 2.11)$$

Where *n* is the diffraction order and θ is the incident angle by the X-rays. The basic geometric derivation of Bragg's Law is illustrated in the following Figure 2.11.

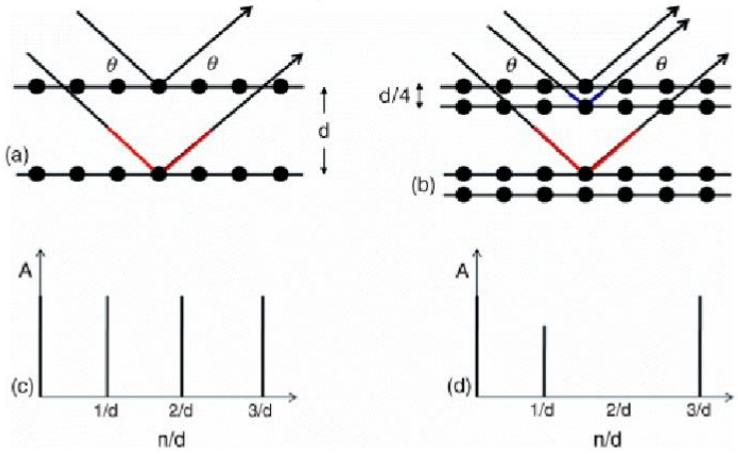

Figure 2.11. Geometric derivation of Bragg's equation for two layers of atoms with interfacial spacing d (a) and idealized amplitude of the scattered waves (c). Also, the effect on an additional layer of atoms at d/4 (b, d) [81].

The result from the amplitude of the diffracted beam as a function of *n/d* or $2\lambda^{-1}sin\theta$ can be plotted as shown in Figure 2.11 (c). In practice, the data is usually plotted against 2θ, normally collected in a 5°-70° range. However, this applies only to an idealized crystal, with no interference from other phases [81]. Conversely, the crystallite size (*d*) can be estimated using Scherrer's equation (Eq. 2.12):

$$d = \frac{K * \lambda}{B * cos\,\theta} \qquad (Eq.\ 2.12)$$

Where *K* is known as shape factor, related to the crystalline shape of the lattice and *B* is the full width at half of the peak in the XRD signal plot, in radians. Cu is a common component of an X-ray source and has a radiation wavelength (CuKα) of 1.5418 Å [82]. The crystallography of the analyzed material will then be compared to the signals received, identifying crystal lattices previously recorded on a database for reference compounds. The most common databases are Powder Diffraction File (PDF) or the International Center for Diffraction Data (ICDD) - JCPDS (Joint Committee on Powder Diffraction Standards).

2.6.2 Temperature Programmed Reduction (TPR)

This technique is used to reduce metal oxides (MO) into metallic compounds, using hydrogen gas at high temperatures and low pressures. It is possible to quantify the oxidation state and the temperature at which the reduction occurs. Furthermore, it can yield information on the degree of reduction, the metallic distribution, and the reducibility of the catalyst. An example of how the reaction proceeds is shown in Eq. 2.13 [82].

$$MO + H_2 \rightleftarrows M\,(metallic) + H_2O \qquad (\text{Eq. } 2.13)$$

Products are the reduced metal (M) and water. As the reaction occurs at high temperatures, the amount of gas absorbed can be deducted from the furnace by a thermal conductivity detector (TCD), since its thermal conductivity is proportional to the mole fraction. Typically, hydrogen gas is dissolved in an inert gas, to facilitate the accuracy of the TCD. Common hydrogen concentrations are 1-10% [82].

2.6.3 Nitrogen Adsorption-Desorption

The adsorption of Nitrogen into porous materials is the most common technique to determine surface area and characterize porosity. Its theoretical foundation is based on the layered sorption of gases, specially physisorption since it occurs at lower adsorption energies, hence there are low structural changes on the absorbant surface. Brunauer, Emmet, and Teller (BET) proposed the layered model in 1938 technically applied to planar surfaces, however, the adsorption process is the same for micropores and mesopores, hence, the procedure is accepted as the standard for calculating the BET surface area [81].

The model is based on the International Union of Pure and Applied Chemistry (IUPAC)'s classification of sorption isotherms, presented in Figure 2.12 (a). The nitrogen adsorption at 77 K and (b) is equivalent to the isotherm I. This curve presents a linear behavior when relative pressure between the equilibrium and the saturation pressure (P/P_0) at a given temperature is between 0.05-0.35. Within the linear behavior region, the BET equation is applied to determine the surface area of porous materials.

$$\frac{1}{W(\frac{P}{P_0}-1)} = \frac{1}{W_m C} + \frac{C-1}{W_m C} * \left(\frac{P}{P_0}\right) \qquad (Eq. 2.14)$$

Where W is the weight of the sample, C is the BET constant related to both absorbent and absorbate. During the measurements, the data is recorded in terms of the term on the left side of Eq. 2.14, hence W_m can be easily solved to determine the surface area.

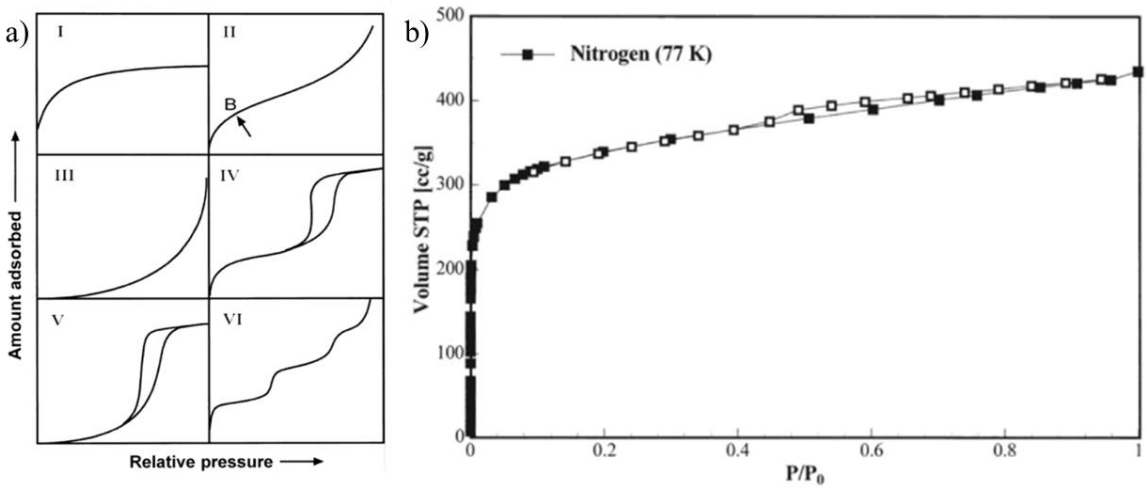

Figure 2.12. a) IUPAC classification of sorption isotherms b) Nitrogen adsorption at 77 K on an active carbon sample, containing micro and mesoporosity indicated by the occurrence of hysteresis at P/P_0. [83]

The approach for determining the pore volume and pore size distribution is referred to as the Barrett-Joyner-Halenda (BJH) method. The capillary condensation region ($P/P_0 > 0,4$), pressure increase causes an increase of the thickness of the layer adsorbed on pore walls, and the capillary condensation in pore having a core size r_c (i.e. pore space) defined by the Kelvin Equation [84], as follows:

$$\ln\left(\frac{P}{P_0}\right) = \frac{-2\gamma w_m cos\theta}{RTr_c} \qquad (Eq.2.15)$$

Where R is the universal constant for gases, T is the temperature, r_c represents the radius for cylindrical pores, γ the surface tension, w_m the molar volume, and θ the contact angle. The assumption of a geometric model allows the calculation of the thickness of the adsorbed film to the total adsorption volume and core volume, followed by estimating the pore volume and pore size, assuming a given pore geometry [84].

2.6.4 N_2O Titration

Since Cu presents the vast majority of active sites for CO_2 hydrogenation to methanol, it is important to have an estimate of the Cu surface area or dispersion while characterizing Cu-based catalysts. Cu surface *dispersion* (D), is defined as the ratio between Cu surface atoms and the total Cu atoms in the catalyst. In Cu-based catalysts, the estimation of metallic Cu

surface area is typically done by the decomposition of nitrogen oxide (N_2O) on the exposed Cu atoms. This process occurs by adsorbing atomic oxygen and releasing gas-phase nitrogen according to the reaction given in Eq. 2.16 [85].

$$N_2O + 2Cu_s \rightarrow (Cu_s - O - Cu_s) + N_2 \qquad \text{(Eq. 2.16)}$$

Where Cu_s represents the metallic Cu exposed on the catalyst's surface. One method of obtaining the Cu surface area is by injecting pulses of N_2O into a reaction set-up with a small amount of the catalyst. The effluent gas composition is then monitored via a thermal conductivity detector (TCD), measuring the amount of both N_2O and N_2. A typical graph of the effluent gas is shown in Figure 2.13, where the mole fraction of the effluent is registered vs reaction time. Using the area under the formed N_2 curve and the mean Cu surface atom density ($1.47x10^{19}$ atoms per m^2), the Cu surface area can be calculated [85]. Other N_2O-based methods have also been proposed (e.g. [86]).

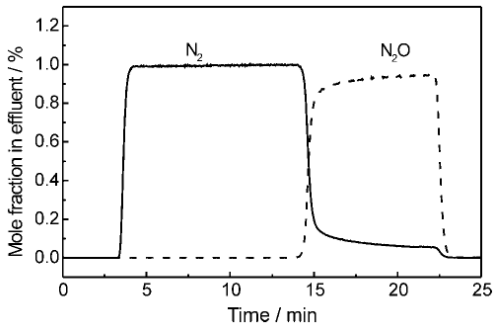

Figure 2.13. N_2O experiment with a $Cu/ZnO/Al_2O_3$ catalyst. Reaction conditions: T = 300K, p = 0.1 MPa, Flow = Nml/min gas misture of 1% N_2O in He [85].

2.6.5 Inductively Coupled Plasma Optical Emission Spectroscopy (ICP-OES)

The ICP-OES is a procedure to determine the metal concentrations present in the catalysts with high accuracy. Its principle is based on a generation of photons of light by the excitation of electrons of a pattern element, generating characteristic wavelength-specific photons emitted by the compounds in the sample [87].

2.6.6 Transmission Electron Microscope (TEM)

Over the last two decades, nanoscale imaging has played a fundamental role in the characterization of heterogeneous catalysts. One of the most common tools to provide detailed information from catalysts is TEM, which uses electrons through the analyzed object to create

a detailed image, to identify structural features. The schematic beam for TEM is depicted in Figure 2.13.

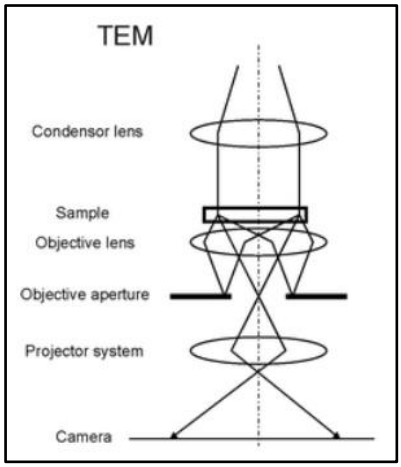

Figure 2.14. Schematic beam path in TEM [88]

TEM provides high-resolution images that allow identifying crystals, pores, metal dispersion, and many other properties. As an example, Figure 2.14 presents a TEM image for a Cu/Si/ZrO catalyst.

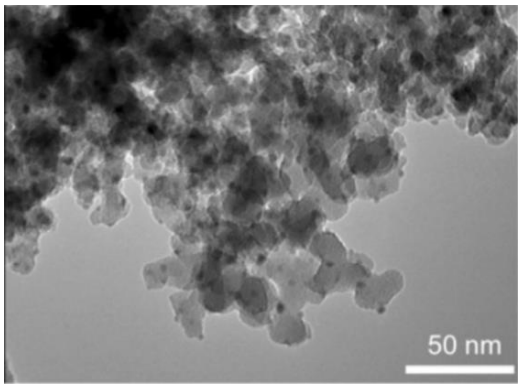

Figure 2.15. TEM image of a Cu/Si/ZrO at 50 nm resolution [89]

2.6.7 Gas Chromatography (GC)

Gas chromatography is by far the most explored technique to quantify catalyst activity for the desired reaction. It is defined by the IUPAC as "*a physical method of separation in which the components to be separated are distributed between two phases: stationary and mobile, the latter moving into a definite direction"* [90]. It uses the diffusion principle to determine the composition of volatile compounds, regardless of their nature.

Samples are vaporized and transported by a carrier gas throughout the chromatographic column. It contains a coating of a stationary phase. The separation of components is determined

by its distribution between the carrier gas and the stationary phase. Different compounds are separated based on their affinity to the stationary phase, measured by their vapor pressure. Information could be further captured by a mass spectrometer (MS), an instrument that measures the mass-to-charge ratio (m/z) and the quantity of a certain type of ions compared to a known m/z ratio, called External Standard (ESTD). Samples are analyzed once they leave the column into a detector, which can be Flame Ionization Detector (FID), Thermoionic Specific Detector (TSD), Flame Photometric Detector (FPD), or Thermal Conductivity Detector (TCD) [91]. Figure 2.15 illustrates the GC/MS system with its major components. Data is captured by a computer system, plotting the response factor (RF) over time for each component in the sample, compared to the calibration curve.

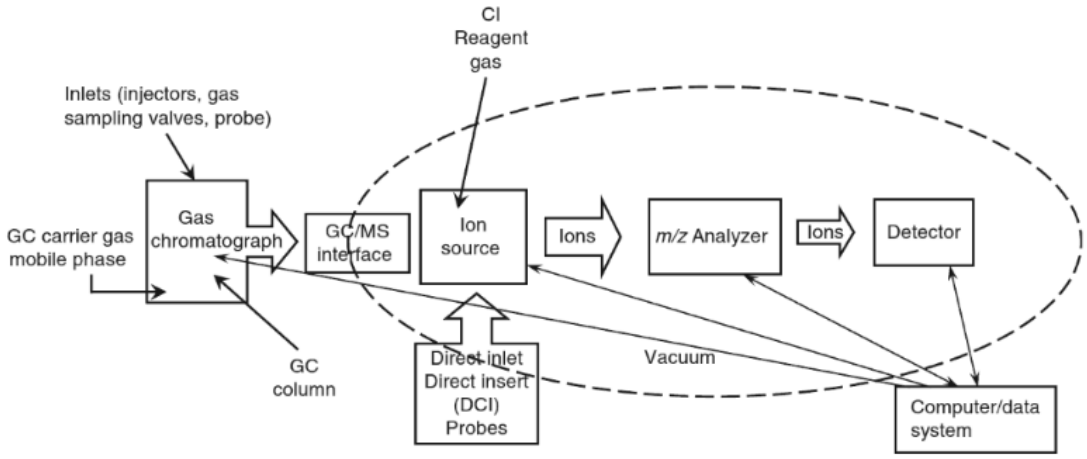

Figure 2.16. Conceptual illustration of the GC/MS system with major components [92].

The following equation is used to calculate the concentration of component i:

$$(Concentration)_i = RF_i * Measured\ Response\ (in\ area\ or\ height)_i$$

Where RF_i is the response factor of i, which is the ratio between the known amount of i and the response of known amount [82]. Information from GC is used to determine catalyst activity: reactants conversion, product selectivity, etc.

3 Experimental

3.1 Catalysts Preparation

Tables 3.1 and 3.2 list the chemicals and gases used to synthesize and test the catalysts in this work.

Table 3.1. List of chemicals used in catalyst synthesis and characterization tests.

No.	Compound	Chemical Formula	Manufacturer	Molecular Weight (g/mol)	Purity
1	Copper (II) nitrate trihydrate	$CuN_2O_6 \cdot 3H_2O$	Acros Organics	241.60	≥99.5%
2	Zinc nitrate hexahydrate	$Zn(NO_3)_2 \cdot 6H_2O$	Alfa Aesar	297.49	≥99.9%
3	Zirconium dinitrate oxide hydrate	$ZrO(NO_3)_2 \cdot 6H_2O$	Alfa Aesar	231.23 (anhy)	≥99.9% (metal basis)
4	Indium (III) nitrate hydrate	$In(NO_3)_3 \cdot xH_2O$	Alfa Aesar	318.83 (anhy)	≥99.99% (metal basis)
5	Sodium hydroxide	NaOH	Emsure	40.00	≥99.2%
6	Sodium carbonate	Na_2CO_3	Emsure	105.99	≥99.9%
7	Silicon carbide	SiC	Alfa Aesar	40.1	≥98.8%
8	Nitric acid (65 %)	HNO_3	VWR Chemicals	63.01	-
9	Hydrochloric acid fuming (37 %)	HCl	Merck	36.46	-

Table 3.2. Gases utilized for catalytic activity tests.

No.	Compound	Chemical Formula	Manufacturer	Molecular Weight (g/mol)	Purity
1	Carbon Dioxide 5.2	CO_2	Yara Praxair	44,01	99.9992%
2	Hydrogen 5.0	H_2	Yara Praxair	2,01	99.999%
3	Nitrogen 5.0	N_2	Yara Praxair	28,01	99.999%
4	Synthetic Air 2.6	$N_2 + O_2$	Yara Praxair	28,96	99.6%

Table 3.3 presents the catalysts prepared in this work. For analysis and characterization, catalysts will be divided by the two main components, i.e., CuZn, CuZr, and CuIn.

Table 3.3. List of synthesized catalysts.

No.	Catalyst	Molar Ratio	Synthesis Method
1	CuZn	Cu:ZnO = 5:1	Coprecipitation
2	In/CuZn	In_2O_3:Cu:ZnO = 0.005:5:1	Wet Impregnation of In_2O_3
3	CuZr	5:1	Coprecipitation
4	In/CuZr	In_2O_3:Cu:ZrO_2 = 0.005:5:1	Wet Impregnation of In_2O_3
5	CuZrIn	Cu:ZrO_2:In_2O_3 = 5:1:0.005	Coprecipitation
6	CuIn	5:1	Coprecipitation
7	Zr/CuIn	ZrO_2:Cu:In_2O_3 = 0.005:5:1	Wet Impregnation of ZrO_2

3.1.1 Synthesis by coprecipitation

A calculated amount of the metal nitrates was dissolved in deionized water (DIW) and vigorously stirred until the compounds were completely dissolved. A second solution containing Na_2CO_3 was prepared. The metal nitrate and sodium carbonate solutions were dropwise combined in a third beaker under continuous stirring such that the pH of the mixture remained constant at ca. 6.5 [49]. In the next step, the solution was aged for 14 h under vigorous stirring at 65 ºC in a sealed cell under a constant flow of N_2. Following the aging process, the precursor slurry was collected using a paper filter of 12-15 µm, washed several times with DIW until the pH of the filtering liquid was 7. The precursor was then dried overnight at 90 ºC before calcination at 300 or 500 °C for 3 hours.

3.1.2 Synthesis by wet impregnation

A calculated amount of metal nitrate and the synthesized bimetallic catalyst was dissolved and dispersed in DIW using ultrasonication until a homogeneous mixture was obtained. The mixture was then covered and stirred overnight at room temperature. Finally, the solution was dried in the oven overnight at 90 ºC before calcination at 350 °C for 3 h.

3.1.3 Calcination procedure

The calcination procedure consisted of placing the precursor in a quartz reactor. The catalysts were calcinated at 350 ºC for 3 hours, with a ramping rate of 2 ºC/min under the flow of synthetic air. After the catalyst was calcinated, a sieving procedure took place to separate grains between 40 – 60 mesh (0,25 – 0,42 mm) for the activity tests.

3.2 Catalysts Characterization

The equipment used and the analysis performed in this work are summarized in Table 3.4.

Table 3.4. Summary of catalyst characterization techniques and the equipment used in this work.

No.	Technique	Device Brand	Model	Property
1	H_2 – TPR	Micrometrics	Autochem II RS232	Reducibility
2	N_2O Titration	Micrometrics	Autochem II RS232	Cu surface area
3	N_2 – Adsorption / Desorption	Micrometrics	TriStar II	Surface area – porosity
4	XRD	Bruker-AXS	D8 Advance	Crystallography
5	ICP	Perkin Elmer	Optima 4300DV	Metal Composition
6	TEM	JEOL	JEM 2100plus	Morphology

3.2.1 Temperature Programmed Reduction (TPR)

H_2-TPR was conducted by an Autochem II analyzer (Table 3.4). First, the samples (about 75 mg) were pretreated at 200 ºC in Helium for 30 minutes to remove traces of water and/or CO_2 in the catalyst. The sample was then cooled to 50 ºC and the flow was switched to 7% H_2/Ar at a flow rate of 50 mL/min. The measurements were done while the temperature was increased from 50 °C to 550 ºC at a rate of 5 ºC/min.

3.2.2 N_2O Titration

A quartz tube was installed into the Autochem II analyzer (Table 3.4). Catalyst samples of ca. 75 mg were treated at 350 ºC for 30 min with 7% H_2/Ar. Next, the reactor was cooled in He flow to room temperature before 1% N_2O/He flowed at 50 mL/min over the sample for 1 h. Then, the sample was purged with He before it was reduced by 7% H_2/Ar. The amount of H_2 used to re-reduce the catalyst was measured. The available Cu surface area was determined by Eq. 3.1[14].

$$S_{Cu} = \frac{n_{Cu} * N_{av}}{W * A} \qquad (Eq. 3.1)$$

Where S_{Cu} is the available Cu surface area per gram catalyst (m^2/g), n_{Cu} is the molar number of Cu, W is the amount of sample, N_{av} is Avogadro's number (6.022×10^{23} atom/mol), and A is the number of Cu atoms per area unit (1.46×10^{19} Cu atom/m^2).

3.2.3 N_2 - Physisorption

Prior to the measurements, the samples were outgassed at 160 °C for 24 h in vacuum using a degassing system (Micrometrics VacPrep 061). N_2 physisorption measurements on the calcined support and catalysts were performed at –196 °C using a Micromeritics Tristar 3000 apparatus. The Brunauer-Emmet-Teller (BET) method was used to calculate the specific surface areas. The pore volumes were determined at P/P_0 = 0.9975. Barrett-Joyner-Halenda (BJH) method analysis (4 V/A) of the desorption branch was used to obtain the pore size distribution.

3.2.4 X-Ray Diffraction (XRD)

The X-ray diffraction (XRD) patterns were recorded for the catalyst precursors and calcined catalysts on a Bruker-AXS Microdiffractometer (D8 ADVANCE) using Cu Kα radiation source (λ = 0.154 nm). The reduced samples were passivated in 1% O_2/N_2 mixture before being transferred to the sample holder. The patterns were collected in the range of 10–90° (2θ) with a step interval of 2°/min. The peaks were indexed according to the database established by the Joint Committee on Powder Diffraction Standards (JCPDS). Figures 3.1 and 3.2 show the precursors and catalysts synthesized in this work, respectively.

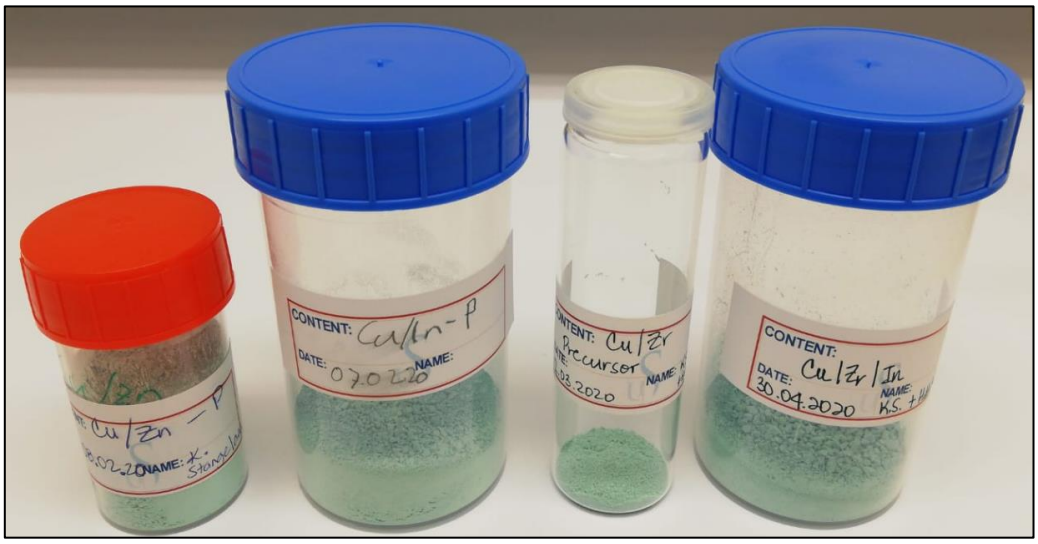

Figure 3.1. Catalysts' precursors listed in Table 3.3.

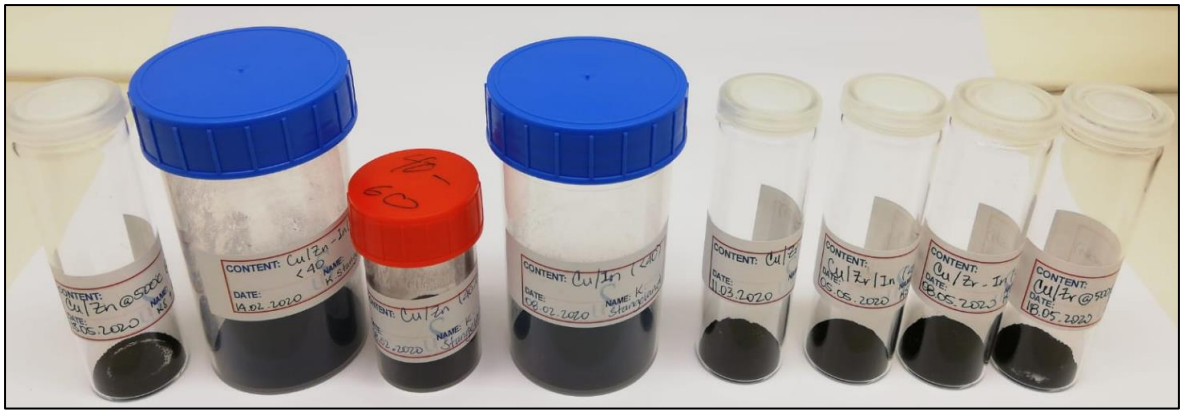

Figure 3.2. Calcinated catalysts listed in Table 3.3.

3.2.5 Inductively Coupled Plasma Optical Emission Spectroscopy (ICP-OES)

To determine the metallic composition of the synthesized catalysts, an ICP-OES procedure was carried out. First, approximately 500 mg of the catalyst was dissolved in 10 ml of Aqua Regia, a solution constituted of nitric acid (HNO_3) and hydrochloric acid (HCl) at a ratio of 1:3. To completely dissolve the catalysts, the mixture was boiled for 30 minutes. The samples were diluted in 25 ml of DIW before analysis. Sample analysis was performed on a *Perkin Elmer Optima 4300DV* spectrometer.

3.2.6 Transmission Electron Microscope (TEM)

The microstructures and morphology of the catalysts were characterized by a transmission electron microscopy (TEM) with a JEOL JEM-2100 F instrument operating at 200 kV. The samples were reduced at 350 °C for 2 h before this analysis and passivated in 1% O_2/N_2. Finally, a small fraction of the catalyst was dispersed in ethanol by ultrasonication and placed into the sample holder.

3.3 Catalysts Activity Tests

The activity tests were conducted with a tubular fixed-bed reactor placed inside an oven. A thermocouple is placed just below the catalyst inside the reactor and the heating temperature is controlled by a regulator (Eurotherm 328). The reactant gases (CO_2, H_2, and N_2) are supplied by three independent lines, each being controlled by a mass flow controller (Bronckhorst). The pressure is controlled by a back-pressure regulator. A complete scheme of this set up is depicted in Figure 3.3, with their corresponding legends for the components. The catalyst was mixed

with SiC before being placed into the reactor on top of a quartz wool plug. The ratio of catalyst to SiC was typically around 1:5.

Before initiating activity tests, the catalysts were reduced for 2 hours at 350 ºC with a temperature rate of 5 ºC/min in a 50% vol H_2/N_2 gas mixture. After reduction, the reactor was purged with N_2 until the temperature was below 50 °C before the reaction mixture was introduced ($H_2/CO_2/N_2$ = 3/1/1). Finally, the pressure was increased to 30 bars, followed by increasing the temperature by 2 ºC/min to the desired reaction temperature established at 230 ºC.

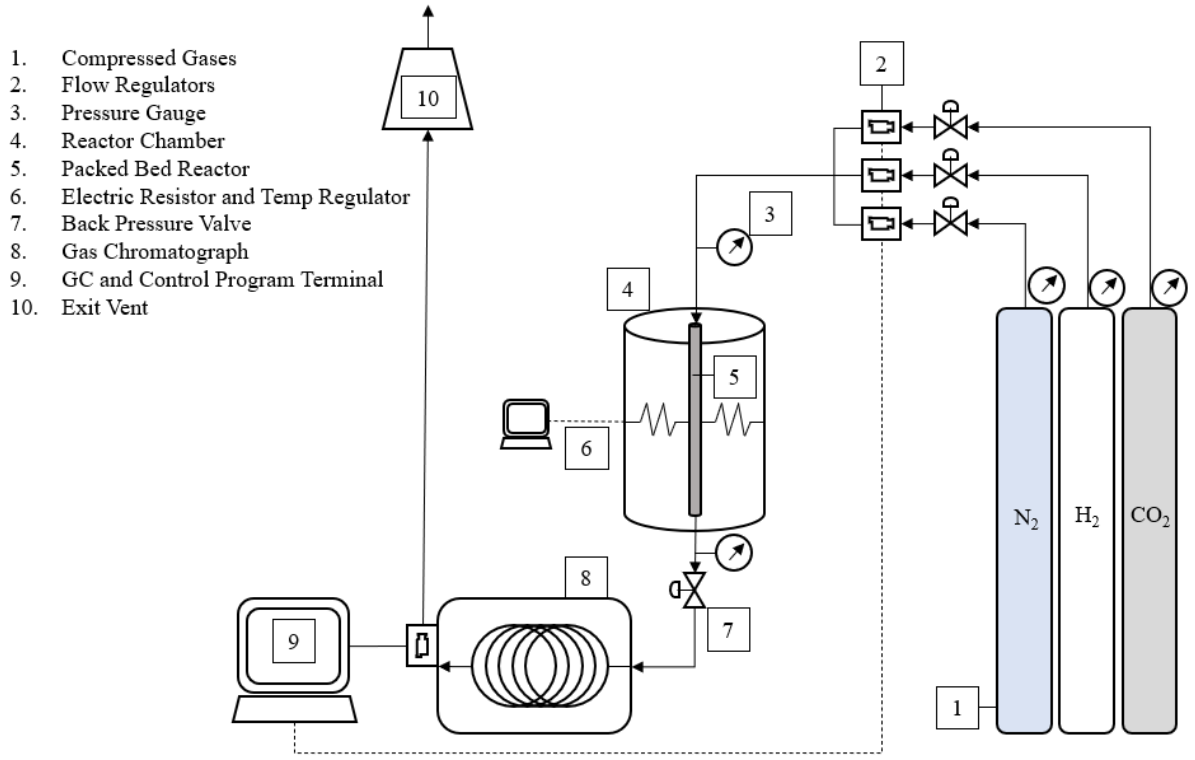

Figure 3.3. Catalysts activity tests set up

The reaction products were analyzed by a Gas Chromatograph (Agilent Technologies 7890B). The CO_2 conversion (X_{CO_2}), and methanol selectivity (S_{CH_3OH}) were calculated based on the Eqs. 3.2 and 3.3, respectively.

$$X_{CO_2} = \frac{n_{CO_2}^{in} - n_{CO_2}^{out}}{n_{CO_2}^{in}} * 100\% \qquad (Eq. 3.2)$$

$$S_{CH_3OH} = \frac{n_{CH_3OH}^{out}}{n_{CO}^{out} + n_{CH_3OH}^{out}} * 100\% \qquad (Eq. 3.3)$$

Where n_i^{in} and n_i^{out} represent the moles of the gas species i at the inlet and outlet streams of the reactor, respectively; F_i the molar flow rate, M_i the molecular weight, and W_{cat} is the weight of the catalysts used for the experiment. Additionally, Space-Time Yield (STY_{CH_3OH}), defined as the quantity of product per unit of volume per unit of time, was calculated using the Eq. 3.4.

$$STY_{CH_3OH} = \frac{F_{CO_2}^{in} * X_{CO_2} * S_{CH_3OH} * M_{CH_3OH}}{W_{cat}} \quad (Eq. 3.4)$$

Where $F_{CO_2}^{in}$ is the molar flow rate and M_{CH_3OH} is the molecular weight of methanol (32.04 gr/mol).

4 Results & Discussion

4.1 Catalyst Characterization

For identification purposes, catalysts will be denoted as in Table 3.2. For instance, CuZn refers to a Cu + ZnO catalyst prepared by coprecipitation, and In/CuZn represents In_2O_3 impregnated on a Cu + ZnO catalyst.

4.1.1 Metal content by ICP-OES

ICP-OES was performed to determine the actual metal content compared to the theoretical concentrations. Table 4.1 shows a comparison between theoretical metal content and the measured metal concentration by ICP-OES.

Table 4.1. Theoretical and measured metal content of different catalysts determined by ICP-OES.

Catalyst	Theoretical molar ratio (%)				Metal content determined by ICP-OES (%)			
	Cu	Zn	Zr	In	Cu	Zn	Zr	In
CuZn	83.3	16.7	–	–	83.2	16.8	–	–
In/CuZn	83.0	16.2	–	0.8	82.1	16.5	–	1.4
CuZr	83.3	–	16.7	–	89.1	–	10.9	
In/CuZr	83.0	–	16.2	0.8	88.0	–	11.0	1.0
CuZrIn	83.0	–	16.2	0.8	88.8	–	11.0	0.2
CuIn	83.3	–	–	16.7	84.1	-	-	15.9
Zr/CuIn	83.0	–	0.8	16.2	Not Available			

- CuZn and In/CuZn catalysts

For the CuZn catalyst, the actual metal concentration obtained by ICP analysis for Cu and Zn was close to the theoretical, meaning the Cu/ZnO was successfully coprecipitated. When In^{3+} was impregnated, the actual amount of In^{3+} was higher than calculated. The value was 1.4% compared to 0.8% molar concentration. This is mostly because the estimated metal content per gram catalysts was higher than the actual values obtained from ICP-OES.

- CuZr, In/CuZr, and CuZrIn catalysts

For the CuZr catalyst, the value after the ICP analysis presented a big deviation from the theoretical content. The expected value of the ZrO_2 was 16.7% compared to the 10.9% obtained. Such a difference can be related to higher crystalline water content in the ZrO_2

compound compared to the value used in the calculations. In addition, a difficult solubilization process was experienced when preparing CuZr catalysts, which could also have affected the ZrO_2 content.

Conversely, similar differences were found with the other two catalysts prepared from Cu and ZrO_2. For the In/CuZr catalyst, the nominal value was 0.8% compared to 1.0% obtained, with minor differences in the Cu and ZrO_2 ratio. Similarly, the CuZrIn catalyst presented a close difference between theoretical In_2O_3 content, 0.2% versus 0.8%, again without significant variation in the Cu and ZrO_2 ratio. It can be concluded that both preparation methods were successful in introducing In_2O_3 into the CuZr catalyst.

- Coprecipitated CuIn catalysts

Only Cu and In were coprecipitated to compare the CuIn catalyst with catalysts containing ZnO and ZrO_2. The value obtained by ICP analysis for Cu and Zn was close to nominal, meaning the CuIn was successfully coprecipitated. Then Zr^{4+} was also impregnated to this catalyst, however, ICP-OES was not performed due to minimal activity of the Zr/CuIn catalyst.

4.1.2 X-Ray Diffraction

- XRD for Catalyst Precursors

XRD patterns of catalysts' precursors are shown in Fig. 4.1. For the CuZn and CuZr, the diffraction peaks were similar to the characteristic peaks of malachite ($Cu_2CO_3(OH)_2$) (PDF 01-072-0075). Peaks at 14.9º, 17.6º, 23.9º, 31.3º, 35.5º are identified, corresponding to (020), (120), (220), $(20\bar{1})$, and (240) planes respectively. Due to their small crystallite size or being amorphous, ZrO_2 and ZnO phases were not detectable. However, the 2θ peak at 31.3º, corresponding to the *d* $(20\bar{1})$ plane is shifted to 32.0º for the CuZn precursor, which can be ascribed to the incorporation of Zn^{2+} into the malachite phase [93].

For the coprecipitated CuIn precursor, besides the peaks of malachite, In^{3+} phases were observed due to the 2θ peak at 22.47º. This corresponds to the (200) plane of $In(OH)_3$, PDF (01-073-1810). The peak at 31.3º is attributed to (220) plane, however, it is overlapped with the malachite phases. As for the coprecipitated CuZrIn precursor, due to the low content of In^{3+}, the representative peaks of $In(OH)_3$ was not identified.

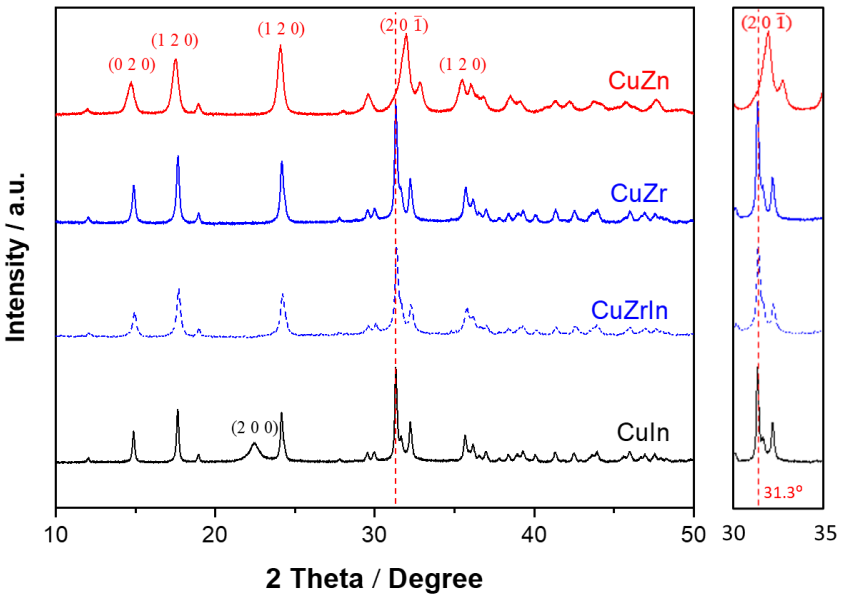

Figure 4.1. X-Ray Diffraction patterns for catalysts' precursors. To the right, an expanded section of the Cu peak (20$\bar{1}$) shifted from 31.3º to 32.0º due to the incorporation of Zn^{2+} into the malachite phase.

- XRD for calcined catalysts

Figure 4.2 presents the XRD patterns for calcined catalysts. Major peaks corresponding to CuO (11$\bar{1}$) and (111) are located at 2θ values of 35.5º and 38.8º, respectively (PDF 00-048-1548). These observations agree with other works [93]. It can be stated that malachite precursors are fully decomposed after calcination at 350 ºC since no other components are reflected in the XRD patterns.

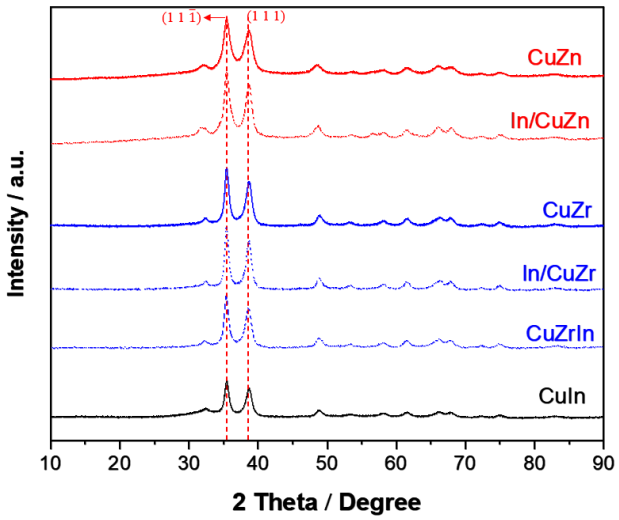

Figure 4.2. XRD patterns for calcined catalysts. Horizontal red lines correspond to peaks at 35.5º and 38.8º, identifying CuO(1 1 1$\bar{1}$) and (1 1 1) planes, respectively.

According to Scherrer's equation (Eq. 2.12), crystallite size is calculated for the calcined catalysts, and the results are presented in Table 4.2. From the values in Table 4.2, it can be seen that the impregnation of In_2O_3 on CuZn increases the crystallite size of CuO from 5.9 to 7.8 nm. This is probably because of the re-calcination at 350 °C, which crystallizes the CuO phase. Similarly, In_2O_3 addition to the CuZr catalyst increases the particle size from 7.9 to 8.8 nm. On the other hand, the crystallite size of CuZrIn (8.2 nm) prepared by co-precipitation is comparable with the CuZr sample.

Table 4.2. Summary of morphological properties of synthesized catalysts. Cu crystallite sizes (dCuO), mean pore sizes, pore volume, BET surface area, and Cu surface area for calcinated catalysts. CuO(111) peak at $2\theta = 38.7^{o}$

Catalyst	d_{CuO} (nm)[a]	Pore Size (nm)[b]	Pore Volume (cm^3/g) [b]	BET Surface Area (m^2/g)[c]	Cu surface area (m^2/g)[d]
CuZn	5.9	7.7	0.17	72	18
In/CuZn	7.8	7.6	0.11	45	17
CuZr	7.8	7.9	0.18	73	34
CuZrIn	8.2	8.8	0.18	77	36
In/CuZr	8.8	9.2	0.15	63	31
CuIn	7.9	7.6	0.19	74	<1

[a] Determined by the Scherrer's equation from XRD data.

[b] Determined using the BJH method, using the peak distribution value for pore size.

[c] Determined by the BET method

[d] Determined by N_2O titration

4.1.3 N_2O Titration

The Cu surface area determined by N_2O titration is also summarized in Table 4.2. Cu surface areas were calculated using the method described in section 2.6.4. and Equation 3.1. The CuZr-based catalysts show the highest Cu surface areas, with values between 31–36 m^2/g, whereas the Cu surface area of the CuZn-based catalysts is around 17–19 m^2/g. This important difference can be supported by previous works, where CuZr catalysts have shown larger Cu surface areas compared to CuZn catalysts [94].

The Cu surface area of CuIn was smaller than 1 m^2/g. This was due to the coverage of surface Cu by In_2O_3 species during the reduction process, since CuIn reduced at 250 °C showed a surface area of 17 m^2/g. In general, there are small differences when comparing the effect of In_2O_3 addition to CuZn or CuZr catalysts. A base value of Cu surface area of 34 m^2/g for the

CuZr catalyst was reduced to 31 m^2/g by wet impregnation and increased slightly to 36 m^2/g when prepared by coprecipitation.

4.1.4 BET surface area

The BET surface area values are shown in Table 4.2. The surface area of the catalysts that were prepared by co-precipitation was similar (72–77 m^2/g), where the CuZrIn catalyst showed the highest BET surface area of 77 m^2/g.

Referring to the addition of In_2O_3, a drop in the BET surface area is observed when the In_2O_3 is added to the catalyst by wet impregnation. The surface area dropped from 72 to 45 m^2/g for the CuZn and 73 to 63 m^2/g for the CuZr. This is probably because of sintering that occurred during the second calcination treatment. The XRD data also indicate that sintering might have occurred. Analyzing the pore sizes, similar pore size is obtained for CuZn, In/CuZn, CuZr, and CuIn around 7.6–7.9 nm. The pore size increased to 8.8 nm for the CuZrIn and was 9.2 nm for the In/CuZr sample.

4.1.5 TEM

A set of images was captured for a group of 5 catalysts. TEM images of CuZn-based catalysts are shown in Figure 4.3, where the scale bar is 100 nm. The morphology and particle size are similar for these catalysts, which are composed of agglomerated particles of ca. 50 nm. The large particles are probably composed of Cu, which is the most abundant species in the catalysts. The smaller particles are typically ZnO, which disperses the Cu phase [42]. For the In/CuZn catalysts, no change in the morphology can be seen after the impregnation of CuZn with In.

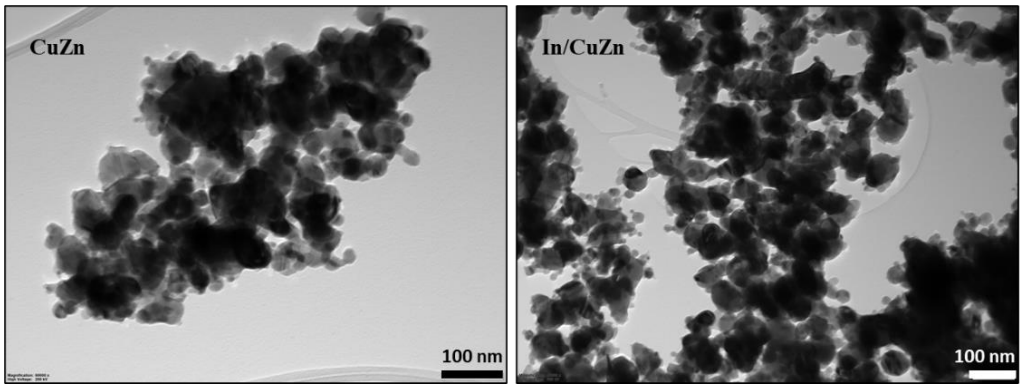

Figure 4.3. TEM images of reduced and passivated CuZn, and In/CuZn catalysts at 100 nm

Figure 4.4 shows the TEM images of CuZr-based catalysts. Certain dense areas can be observed in CuZr and In/CuZr, which could be caused by a more significant agglomeration of Cu phases. The morphology is relatively similar to that of CuZn-based catalysts with comparable Cu particle size. Very small particles can be seen in CuZr, In/CuZr, and CuZrIn, which can be attributed to ZrO_2. This is supported by the fact that ZrO_2 phases are not detected by XRD. Furthermore, similar structures have been observed by other studies [58], [95].

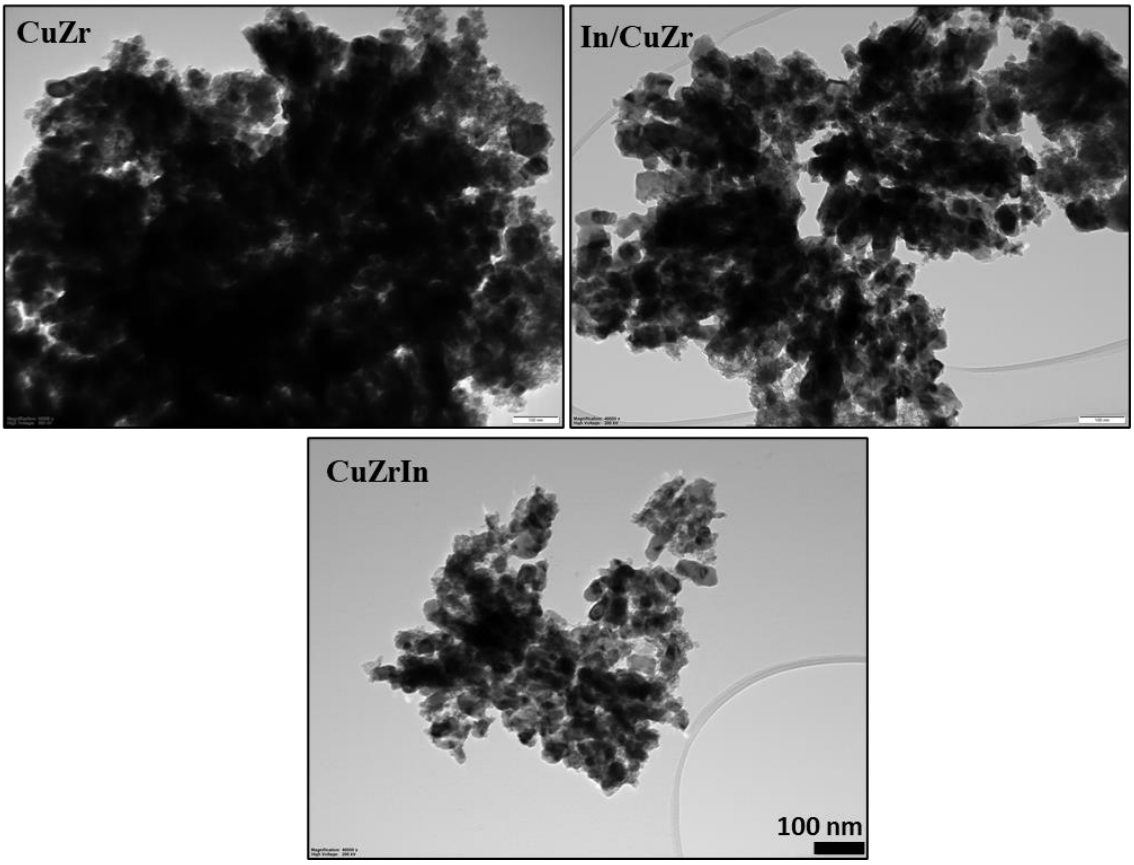

Figure 4.4. TEM images of reduced and passivated CuZr-based catalysts (scale bar is 100 nm).

A comparison of the metal oxide phase between In/CuZr and CuZn is shown in Figure 4.5. It can be observed that a group of much smaller particles exist in the In/CuZr sample that can not be observed in the CuZn catalyst. The same observation was made by Natesakhawat et al. [38], comparing CuZnZrGaY with a CuZn catalyst.

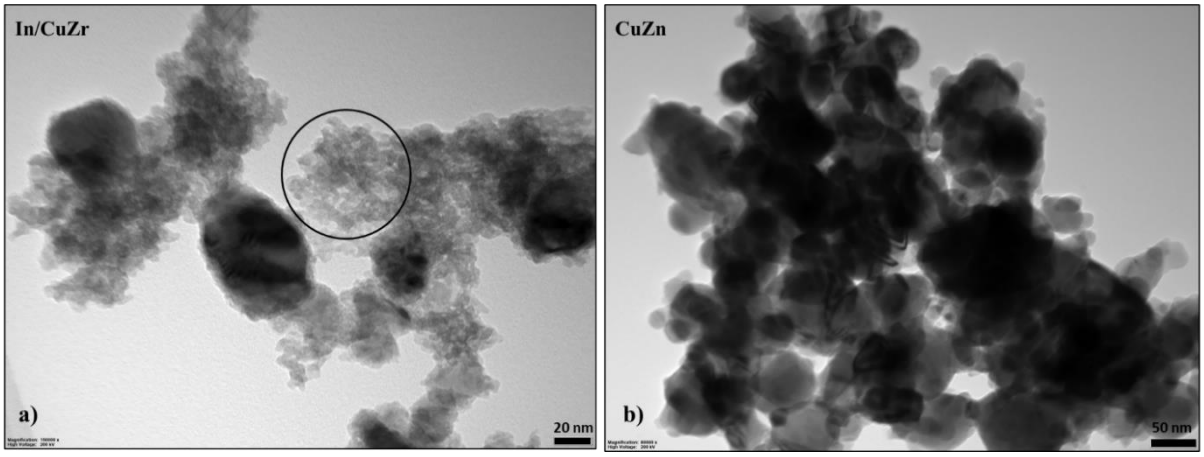

Figure 4.5. a) TEM image of In/CuZr catalyst. Small crystals enclosed in the circle attributed to the ZrO2. b) A TEM image from CuZn, where no small particles can be identified.

4.1.6 Temperature Programmed Reduction (TPR)

The H_2-TPR profiles are presented in Figure 4.6. All catalysts show a similar reduction pattern and are fully reduced below 200 °C.

- Reducibility of bimetallic catalysts (CuZn, CuIn, CuZr)

The most intense peak appearing at 150–175 °C (β) is ascribed to highly dispersed CuO species, while the shoulder (γ) at 160–190 °C is attributed to bulk CuO. A third weak peak (α) can be observed for ZrO_2 containing samples. This is related to the interaction between highly dispersed Cu species and the support when ZrO_2 is present, supported by other studies [93, 95]. It can also be seen that CuO is more easily reduced when ZrO_2 is present compared to ZnO or In_2O_3, as (β) and (γ) peaks are located at lower temperatures compared to CuZn and CuIn.

- Influence of In_2O_3

When In_2O_3 is added to the catalyst by wet impregnation, the reduction profile shifts towards higher temperatures, which can be ascribed to more stable CuO species. The increased stability of the CuO species might be due to larger particles or increased crystallinity as well as weakened metal-support interaction. To some extent, this can be attributed to the second calcination cycle at 350 °C since the reducibility is similar for the CuZr and CuZrIn catalysts.

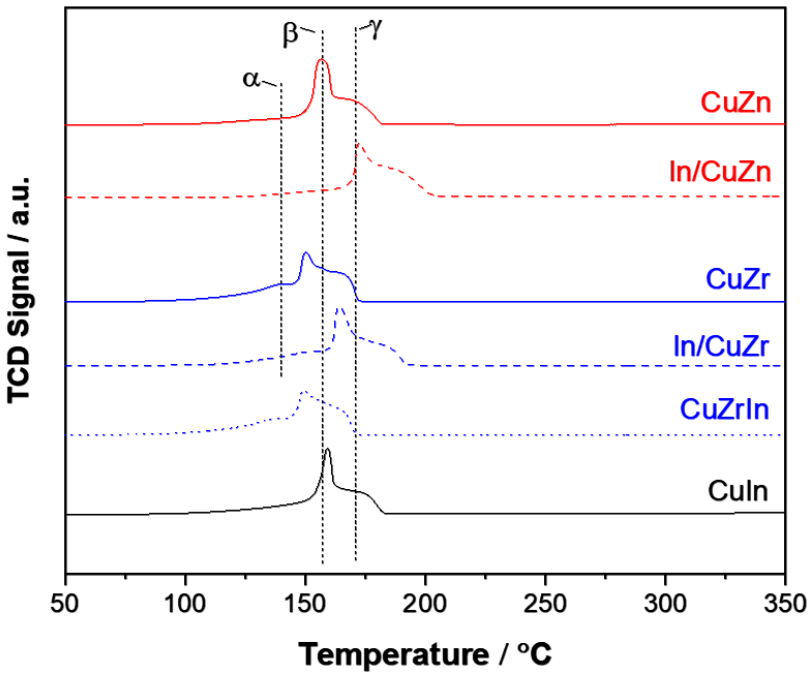

Figure 4.6. H_2-TPR profiles of calcined catalysts. Peaks (β) and (γ) are referenced against CuZn, while (α) peak is referenced by CuZr.

4.2 Methanol Synthesis Activity

4.2.1 Activity tests at 230 °C

All the catalysts synthesized were tested for CO_2 conversion to methanol. Figure 4.7 depicts the methanol selectivity at different CO_2 conversions, calculated by using Eq. 3.2 and 3.3. The CO_2 conversion was varied by changing the gas space hourly velocity (GSHV) from 3600 to 9800 mL/(g_{cat} h).

It can be seen that the methanol selectivity increased for all catalysts when the GHSV was increased. This is expected as the methanol synthesis reaction is faster than the RWGS reaction at the conditions used in this work. A similar effect of contact time on the methanol selectivity has also been reported by Tada et al. [58].

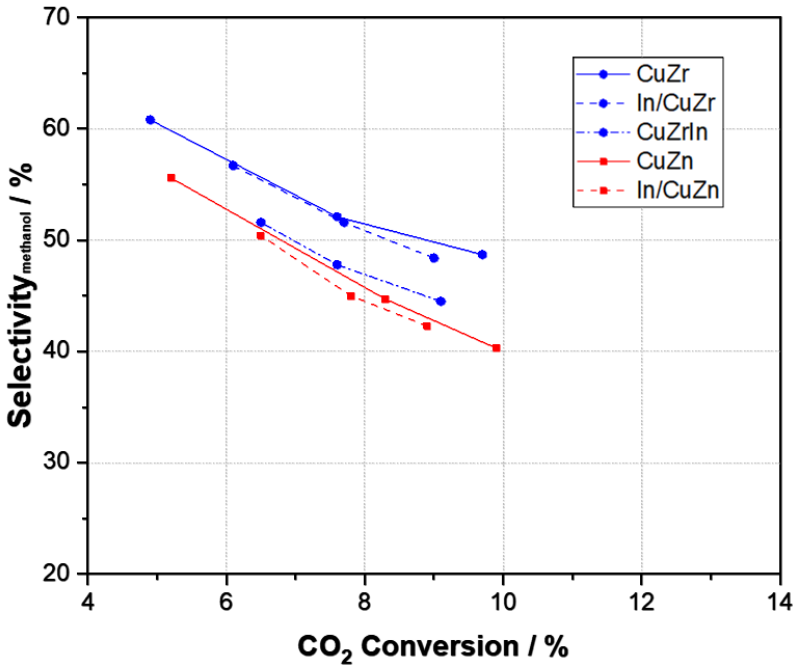

Figure 4.7. CO_2 conversion (%) vs. Methanol Selectivity (%) for calcinated catalysts.

- Comparison of CuZn and CuZr catalysts

There is a significant difference in the methanol selectivity when CuZn and CuZr catalysts are compared. It can be seen that the trendline appears at higher methanol selectivity for CuZr compared to CuZn. This indicates that the active sites generated on CuZr are more suitable for CO_2 hydrogenation to methanol than Cu/ZnO. The results over different catalysts at 230 °C and a CO_2 conversion of ca. 8% are shown in Table 4.3. For CO_2 conversions around 8%, the methanol selectivity of CuZn was 44.7%, whereas the selectivity was 52.1% for CuZr. However, the methanol production rate was significantly higher for CuZn. The CuZn catalyst exhibited a rate of 523 mg/(g_{cat} h), while the rate over CuZr was 420 mg/(g_{cat} h). This is attributed to a higher amount of interfacial sites in CuZn compared to CuZr.

The following observations support this conclusion: (i) CuZr contains a lower CuZr ratio; (ii) dense areas are observed by TEM for CuZr indicating separation, which is not observed for CuZn, and (iii) the Cu surface area is higher for CuZr than CuZn, indicating the important role of the interfacial sites as shown by other research groups [52, 53, 56].

Table 4.3. Catalytic performance of different catalysts at 230 °C.

Catalyst	CO_2 conversion (%)	Methanol selectivity (%)	$STY_{methanol}$ ($mg_{methanol}\ g_{cat}^{-1}\ h^{-1}$)
CuZn	8.3	44.7	523
In/CuZn	7.8	45.0	322
CuZr	7.6	52.1	420
CuZrIn	7.6	47.8	329
In/CuZr	7.7	51.6	340

- Influence of In_2O_3

For the CuZn catalysts, there is no significant change in the methanol selectivity trendline when In_2O_3 is added via impregnation (Figure 4.7). However, it can be seen from Table 4.2 that the STY of methanol decreases from 523 to 322 mg/(g_{cat} h). Comparing the CuZr and In/CuZr catalysts, the effect is similar as for In addition to CuZn, where the STY of methanol drops from 420 to 329 mg/(g_{cat} h). On the contrary, there is a noticeable decline in the methanol selectivity when In_2O_3 was incorporated via coprecipitation. It can be seen from Figure 4.7 that the trendline of CuZrIn appears at lower values compared to CuZr and In/CuZr. Furthermore, CuZrIn exhibits a STY of methanol of only 329 mg/(g_{cat} h).

The drop in STY of methanol is attributed to the blockage of active sites by In_2O_3. This is supported by the fact that CuIn and Zr/CuIn showed very low activity at 230 °C (too low activity to accurately determine it). Additionally, the Zr/CuIn catalyst showed some initial activity when reduced at 250 °C, but deactivated rapidly within the first hour and was eventually completely inactive. This is attributed to the migration of In_2O_3 species that covers the Cu surface, which is supported by the N_2O results obtained for CuIn reduced at different temperatures.

- Correlating activity to the Cu surface area

To compare the activity of the catalysts, the STY per Cu surface area was calculated for each of the tested catalysts. The STY per surface area Cu is plotted against the Cu surface area in Figure 4.8. No correlation between the activity and the Cu surface area is obtained for the catalysts investigated in this work at 230 °C. It can be seen that the CuZn and In/CuZn shows the highest methanol formation rate per Cu surface area. Although CuZr, In/CuZr, and CuZrIn

show significantly higher Cu surface area, the activity per Cu surface area of these catalysts is much lower than that of CuZn and In/CuZn. It is likely that a significant portion of the Cu is not in proximity to ZrO_2 and therefore, not particularly active for methanol synthesis [96]. In agreement, Wang et al. [54] also concluded that larger Cu surface areas do not imply higher catalytic activity.

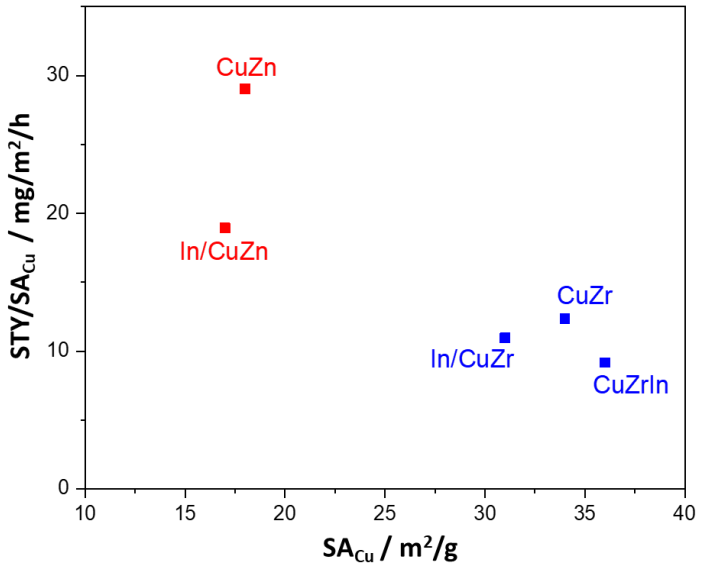

Figure 4.8. Cu Surface Area vs. Space-Time Yield/SACu for all selected catalysts.

When In_2O_3 is added to the CuZn and CuZr by impregnation, the activity decreases significantly. This has also been reported by other researchers [17], [19]. The second calcination procedure at 350 °C for 3h after wet impregnation on In/CuZn and In/CuZr catalysts might also have resulted in lower activity due to sinter of the Cu and metal oxide phases.

4.2.2 Activity tests at 270 °C

- Comparing CuZn and CuZr

The results over different catalysts at 270 °C and a CO_2 conversion of 6.9–8.1% are shown in Table 4.4. Comparing the CuZn and CuZr catalyst, the selectivity of the CuZr catalyst is higher (27.9%) than that of CuZn (10.0%). Furthermore, a STY of methanol of 931 mg/(g_{cat} h) is obtained over CuZr, which is almost 4 times higher than that of CuZn at 268 mg/(g_{cat} h). This further supports that the active sites of CuZr are more favorable for methanol production compared to the active sites on CuZn.

Table 4.4. Catalytic performance at 270 °C of different catalysts.

Catalyst	CO_2 conversion (%)	Methanol selectivity (%)	$STY_{methanol}$ ($mg_{methanol}\ g_{cat}^{-1}\ h^{-1}$)
CuZn	6.9	10.0	268
In/CuZn	7.1	10.8	174
CuZr	7.8	27.9	931
CuZrIn	7.4	32.2	971
In/CuZr	8.1	38.9	449

- Effect of In_2O_3

The effect of In_2O_3 addition to CuZn has no noticeable effect on the selectivity of the catalyst at similar CO_2 conversion. Similar to the results at 230 °C, a drop in the STY of methanol is still observed at 270 °C from 268 mg/(g_{cat} h) for CuZn to 174 mg/(g_{cat} h) for In/CuZn. In contrast, an improvement in methanol selectivity can be seen for In_2O_3 addition to CuZr. The highest methanol selectivity at 270 °C of 38.9% is obtained over In/CuZr. Furthermore, the STY of methanol is higher for CuZrIn at 971 mg/(g_{cat} h) than CuZr (931 mg/(g_{cat} h)). These results suggest that In_2O_3 species are involved in the active site when In_2O_3 is combined with CuZr. In addition, since the methanol selectivity was not improved for In_2O_3 addition to CuZn, the results suggest that a synergistic effect between ZrO_2 and In_2O_3 species is present. However, the In_2O_3-ZrO_2 sites appear to require a higher temperature to be active, which is also typically the case for In_2O_3-based catalysts [16] [63] [64].

A similar conclusion has also been reported by Yao et al. for CuZrIn catalysts [18],where defective In_2O_3 sites enhanced CO_2 adsorption and methanol selectivity. The CuZrIn catalysts investigated in this work could have potential as a selective catalyst at high temperatures. However, further work is required to optimize the catalyst.

5 Conclusions

The present work evaluated the characteristics and the catalytic performance of In_2O_3-promoted CuZn and CuZr for CO_2 hydrogenation to methanol. In_2O_3-containing catalysts were prepared via wet impregnation and coprecipitation methods. Several procedures were carried out to evaluate the physicochemical and textural features of the catalysts, such as XRD, H_2-TPR, TEM, ICP-OES, N_2O titration, and N_2 physisorption.

The main conclusions from the systematic catalyst characterization can be summarized as in the following:

- Malachite precursors can fully decompose after calcination at 350 ºC, and it is the predominant crystalline structure for the catalysts synthesized in this work.
- Adding In_2O_3 leads to an increase in the crystallite size of Cu-based catalysts.
- The highest Cu surface area is obtained for CuZr compared to CuIn and CuZn.
- In_2O_3 increases the reduction temperature for CuO. The opposite effect is caused by ZrO_2, which leads to a lower reducing temperature.
- N_2O titration indicates that In_2O_3 species migrate to the Cu surface at relatively low temperatures.

The activity tests showed that CO_2 conversion, selectivity, and STY were different for CuZn- and CuZr-based catalysts:

- There is no significant effect when In_2O_3 was added to Cu-based catalysts via wet impregnation method under the experimental conditions performed in this work. On the other hand, there is a clear reduction in the catalytic activity when In_2O_3 is synthesized by coprecipitation.
- CuZn and CuZr - based catalysts present relatively similar activity for the reaction conditions of the experiment, with CO_2 conversion values around 8% and methanol selectivities between 45-55%. Experimental values showed CuZr catalysts yield higher methanol selectivity values compared to CuZn catalysts.
- Despite a smaller Cu surface area for CuZn catalysts, the catalytic activity per Cu surface area is 2-3 times higher for CuZn catalysts than the CuZr catalysts at 230 °C
- CuZr catalysts show better performance than CuZn at 270 °C
- CuIn and Zr/CuIn are not particularly active for the reaction conditions carried out in this work, probably because of significant coverage of Cu by In_2O_3.

- In_2O_3 reduced the catalytic activity per Cu surface area at 230 °C, regardless of the synthesis method for Cu-based catalysts.
- In_2O_3 can enhance the methanol selectivity and the STY of methanol at 270 °C for CuZr, whereas it only lowers the activity of CuZn

5.1 Future Work Recommendations

Utilizing In_2O_3 can enhance the performance of CuZr-based catalysts at high reaction temperatures. One of the challenges is that In_2O_3 will migrate and cover the Cu surface at high In_2O_3 content and deactivate the catalysts. Thus, it could be a promising catalyst for high-temperature applications if In_2O_3 could be stabilized in proximity to ZrO_2.

It is necessary to investigate the In_2O_3 to ZrO_2 ratio to avoid coverage of Cu species. More work regarding stability is also required. The limited investigations and the lack of a solid consensus on the catalytic activity of In_2O_3 for CO_2 hydrogenation to methanol are yet other drivers for carrying out investigations on its promotional effects over Cu-based catalytic systems.

References

[1] D. Coley, *Energy and climate change: creating a sustainable future*. John Wiley & Sons, 2011.

[2] W. Kuckshinrichs and J.-F. Hake, *Carbon Capture, Storage and Use: Technical, Economic, Environmental and Societal Perspectives.* Springer, 2015.

[3] T. F. Stocker *et al.*, "Climate change 2013: The physical science basis," *Contribution of working group I to the fifth assessment report of the intergovernmental panel on climate change*, vol. 1535, 2013.

[4] G. Centi and S. Perathoner, *Green carbon dioxide: advances in CO2 utilization*. John Wiley & Sons, 2014.

[5] I. E. Agency, "Exploring Clean Energy pathways – The Role of CO2 Storage," July 2019 2019. [Online]. Available: https://webstore.iea.org/exploring-clean-energy-pathways

[6] G. A. Olah, "Beyond Oil and Gas: The Methanol Economy," *Angew. Chem. Int. Ed*, vol. 44, pp. 2636-2639, 2005.

[7] W.-C. Liu, J. Baek, and G. A. Somorjai, "The methanol economy: methane and carbon dioxide conversion," *Topics in Catalysis*, vol. 61, no. 7-8, pp. 530-541, 2018.

[8] "The Methanol Institute." https://www.methanol.org/uses/ Accessed: 15.05.2020.

[9] X. Jiang, X. Nie, X. Guo, C. Song, and J. G. Chen, "Recent Advances in Carbon Dioxide Hydrogenation to Methanol via Heterogeneous Catalysis," *Chemical Reviews*, 2020.

[10] M. Alvarado, "Methanol Industry Overview," *Opportunities and Challenges for Methanol as a Global Liquid Energy Carrier*, 2017.

[11] G. A. Olah, A. Goeppert, and G. S. Prakash, *Beyond oil and gas: the methanol economy*. John Wiley & Sons, 2018.

[12] W. Li *et al.*, "A short review of recent advances in CO 2 hydrogenation to hydrocarbons over heterogeneous catalysts," *RSC advances*, vol. 8, no. 14, pp. 7651-7669, 2018.

[13] J. T. Sun, I. S. Metcalfe, and M. Sahibzada, "Deactivation of Cu/ZnO/Al2O3 methanol synthesis catalyst by sintering," *Industrial & engineering chemistry research*, vol. 38, no. 10, pp. 3868-3872, 1999.

[14] P. Gao *et al.*, "Influence of modifier (Mn, La, Ce, Zr and Y) on the performance of Cu/Zn/Al catalysts via hydrotalcite-like precursors for CO2 hydrogenation to methanol," *Applied Catalysis A: General*, vol. 468, pp. 442-452, 2013.

[15] J. Ye, C. Liu, D. Mei, and Q. Ge, "Active oxygen vacancy site for methanol synthesis from CO2 hydrogenation on In2O3 (110): a DFT study," *ACS Catalysis*, vol. 3, no. 6, pp. 1296-1306, 2013.

[16] K. Sun *et al.*, "Hydrogenation of CO2 to methanol over In2O3 catalyst," *Journal of CO2 Utilization*, vol. 12, pp. 1-6, 2015.

[17] J. Słoczyński *et al.*, "Effect of metal oxide additives on the activity and stability of Cu/ZnO/ZrO2 catalysts in the synthesis of methanol from CO2 and H2," *Applied Catalysis A: General*, vol. 310, pp. 127-137, 2006.

[18] L. Yao, X. Shen, Y. Pan, and Z. Peng, "Synergy between active sites of Cu-In-Zr-O catalyst in CO2 hydrogenation to methanol," *Journal of Catalysis*, vol. 372, pp. 74-85, 2019.

[19] M. Sadeghinia, M. Rezaei, A. N. Kharat, M. N. Jorabchi, B. Nematollahi, and F. Zareiekordshouli, "Effect of In2O3 on the structural properties and catalytic performance of the CuO/ZnO/Al2O3 catalyst in CO2 and CO hydrogenation to methanol," *Molecular Catalysis*, vol. 484, p. 110776, 2020.

[20] A. A. Vertès, N. Qureshi, H. Yukawa, and H. P. Blaschek, *Biomass to biofuels: strategies for global industries*. John Wiley & Sons, 2011.
[21] A. Basile and F. Dalena, *Methanol: Science and Engineering*. Elsevier, 2017.
[22] D. Sheldon, "Methanol Production-A Technical History," *Johnson Matthey Technology Review*, vol. 61, no. 3, pp. 172-182, 2017.
[23] G. Natta, "Synthesis of Methanol in Catalysis Vol. 3," ed: Reinhold Publishing Corporation, New York, 1955.
[24] S. Lee, *Methanol synthesis technology*. CRC press, 1989.
[25] P. Tijm, F. Waller, and D. Brown, "Methanol technology developments for the new millennium," *Applied Catalysis A: General*, vol. 221, no. 1-2, pp. 275-282, 2001.
[26] K. Westerterp, "New methanol processes," in *Energy Efficiency in Process Technology*: Springer, 1993, pp. 1142-1153.
[27] D. S. Marlin, E. Sarron, and Ó. Sigurbjörnsson, "Process advantages of direct CO2 to methanol synthesis," *Frontiers in chemistry*, vol. 6, p. 446, 2018.
[28] E. Ng, L. Berton, and M. Hogan. "Feature: Coronavirus outbreak leaves outlook for global methanol markets mixed." S&P Global. https://www.spglobal.com/platts/en/market-insights/latest-news/petrochemicals/020520-feature-coronavirus-outbreak-leaves-outlook-for-global-methanol-markets-mixed Accessed: 10.05.2020.
[29] A. Gedde-Dahl, K. J. Kristiansen, H. Holm-Larsen, and H. Topsøe, "The 2,400 MTPD Methanol Plant at Tjeldbergodden," in *World Methanol Conference*, 1998.
[30] K. Stangeland, H. Li, and Z. Yu, "Thermodynamic analysis of chemical and phase equilibria in CO2 hydrogenation to methanol, dimethyl ether, and higher alcohols," *Industrial & Engineering Chemistry Research*, vol. 57, no. 11, pp. 4081-4094, 2018.
[31] G. Leonzio, E. Zondervan, and P. U. Foscolo, "Methanol production by CO2 hydrogenation: analysis and simulation of reactor performance," *International Journal of Hydrogen Energy*, vol. 44, no. 16, pp. 7915-7933, 2019.
[32] C. V. Miguel, M. A. Soria, A. Mendes, and L. M. Madeira, "Direct CO2 hydrogenation to methane or methanol from post-combustion exhaust streams–A thermodynamic study," *Journal of Natural Gas Science and Engineering*, vol. 22, pp. 1-8, 2015.
[33] S. Kattel, P. J. Ramírez, J. G. Chen, J. A. Rodriguez, and P. Liu, "Active sites for CO2 hydrogenation to methanol on Cu/ZnO catalysts," *Science*, vol. 355, no. 6331, pp. 1296-1299, 2017.
[34] O. A. Ojelade and S. F. Zaman, "A Review on Pd Based Catalysts for CO 2 Hydrogenation to Methanol: In-Depth Activity and DRIFTS Mechanistic Study," *Catalysis Surveys from Asia*, vol. 24, no. 1, pp. 11-37, 2020.
[35] F. Studt *et al.*, "The mechanism of CO and CO2 hydrogenation to methanol over Cu-based catalysts," *ChemCatChem*, vol. 7, no. 7, pp. 1105-1111, 2015.
[36] T. Kakumoto, "A theoretical study for the CO2 hydrogenation mechanism on Cu/ZnO catalyst," *Energy conversion and management*, vol. 36, no. 6-9, pp. 661-664, 1995.
[37] M. Spencer, "Role of ZnO in methanol synthesis on copper catalysts," *Catalysis letters*, vol. 50, no. 1-2, pp. 37-40, 1998.
[38] S. Natesakhawat *et al.*, "Active sites and structure–activity relationships of copper-based catalysts for carbon dioxide hydrogenation to methanol," *ACS Catalysis*, vol. 2, no. 8, pp. 1667-1676, 2012.
[39] J. Nakamura *et al.*, "Methanol synthesis over a Zn-deposited copper model catalyst," *Catalysis letters*, vol. 31, no. 4, pp. 325-331, 1995.
[40] T. Fujitani, I. Nakamura, T. Uchijima, and J. Nakamura, "The kinetics and mechanism of methanol synthesis by hydrogenation of CO2 over a Zn-deposited Cu (111) surface," *Surface science*, vol. 383, no. 2-3, pp. 285-298, 1997.

[41] M. Behrens *et al.*, "The active site of methanol synthesis over Cu/ZnO/Al2O3 industrial catalysts," *Science*, vol. 336, no. 6083, pp. 893-897, 2012.
[42] A. Karelovic and P. Ruiz, "The role of copper particle size in low pressure methanol synthesis via CO 2 hydrogenation over Cu/ZnO catalysts," *Catalysis Science & Technology*, vol. 5, no. 2, pp. 869-881, 2015.
[43] R. Van Den Berg *et al.*, "Structure sensitivity of Cu and CuZn catalysts relevant to industrial methanol synthesis," *Nature communications*, vol. 7, no. 1, pp. 1-7, 2016.
[44] D. Gasser and A. Baiker, "Hydrogenation of carbon dioxide over copper—zirconia catalysts prepared by in-situ activation of amorphous copper—zirconium alloy," *Applied catalysis*, vol. 48, no. 2, pp. 279-294, 1989.
[45] N. Kanoun, M. Astier, and G. Pajonk, "Catalytic properties of new Cu based catalysts containing Zr and/or V for methanol synthesis from a carbon dioxide and hydrogen mixture," *Catalysis letters*, vol. 15, no. 3, pp. 231-235, 1992.
[46] Y. Nitta, O. Suwata, Y. Ikeda, Y. Okamoto, and T. Imanaka, "Copper-zirconia catalysts for methanol synthesis from carbon dioxide: Effect of ZnO addition to Cu-ZrO 2 catalysts," *Catalysis letters*, vol. 26, no. 3-4, pp. 345-354, 1994.
[47] T. C. Schilke, I. A. Fisher, and A. T. Bell, "In SituInfrared Study of Methanol Synthesis from CO2/H2on Titania and Zirconia Promoted Cu/SiO2," *Journal of Catalysis*, vol. 184, no. 1, pp. 144-156, 1999.
[48] K. T. Jung and A. T. Bell, "Effects of zirconia phase on the synthesis of methanol over zirconia-supported copper," *Catalysis letters*, vol. 80, no. 1-2, pp. 63-68, 2002.
[49] F. Arena *et al.*, "Solid-state interactions, adsorption sites and functionality of Cu-ZnO/ZrO2 catalysts in the CO2 hydrogenation to CH3OH," *Applied Catalysis A: General*, vol. 350, no. 1, pp. 16-23, 2008.
[50] K. Samson *et al.*, "Influence of ZrO2 structure and copper electronic state on activity of Cu/ZrO2 catalysts in methanol synthesis from CO2," *ACS Catalysis*, vol. 4, no. 10, pp. 3730-3741, 2014.
[51] T. Witoon, J. Chalorngtham, P. Dumrongbunditkul, M. Chareonpanich, and J. Limtrakul, "CO2 hydrogenation to methanol over Cu/ZrO2 catalysts: Effects of zirconia phases," *Chemical Engineering Journal*, vol. 293, pp. 327-336, 2016.
[52] S. Tada *et al.*, "Cu species incorporated into amorphous ZrO2 with high activity and selectivity in CO2-to-methanol hydrogenation," *The Journal of Physical Chemistry C*, vol. 122, no. 10, pp. 5430-5442, 2018.
[53] I. Ro *et al.*, "The role of the Cu-ZrO2 interfacial sites for ethanol conversion to ethyl acetate and methanol synthesis from CO2 and H2," *ACS Catal*, vol. 6, no. 7040-7050, p. 12, 2016.
[54] Y. H. Wang, W. G. Gao, H. Wang, Y. E. Zheng, W. Na, and K. Z. Li, "Structure–activity relationships of Cu–ZrO 2 catalysts for CO 2 hydrogenation to methanol: interaction effects and reaction mechanism," *RSC advances*, vol. 7, no. 14, pp. 8709-8717, 2017.
[55] K. Larmier *et al.*, "CO2-to-methanol hydrogenation on zirconia-supported copper nanoparticles: reaction intermediates and the role of the metal–support interface," *Angewandte Chemie International Edition*, vol. 56, no. 9, pp. 2318-2323, 2017.
[56] K. Fujiwara, S. Tada, T. Honma, H. Sasaki, M. Nishijima, and R. Kikuchi, "Influences of particle size and crystallinity of highly loaded CuO/ZrO2 on CO2 hydrogenation to methanol," *AIChE Journal*, vol. 65, no. 12, p. e16717, 2019.
[57] K. Li and J. G. Chen, "CO2 hydrogenation to methanol over ZrO2-containing catalysts: Insights into ZrO2 induced synergy," *ACS Catalysis*, vol. 9, no. 9, pp. 7840-7861, 2019.
[58] S. Tada *et al.*, "Ag addition to CuO-ZrO2 catalysts promotes methanol synthesis via CO2 hydrogenation," *Journal of Catalysis*, vol. 351, pp. 107-118, 2017.

[59] A. M. Hengne *et al.*, "Ni–Sn-supported ZrO2 catalysts modified by indium for selective CO2 hydrogenation to methanol," *ACS omega*, vol. 3, no. 4, pp. 3688-3701, 2018.
[60] P. Clancy, J. P. Breen, and J. R. Ross, "The preparation and properties of coprecipitated Cu–Zr–Y and Cu–Zr–La catalysts used for the steam reforming of methanol," *Catalysis today*, vol. 127, no. 1-4, pp. 291-294, 2007.
[61] B. Lindström, L. J. Pettersson, and P. G. Menon, "Activity and characterization of Cu/Zn, Cu/Cr and Cu/Zr on γ-alumina for methanol reforming for fuel cell vehicles," *Applied catalysis A: general*, vol. 234, no. 1-2, pp. 111-125, 2002.
[62] O. Martin *et al.*, "Indium oxide as a superior catalyst for methanol synthesis by CO2 hydrogenation," *Angewandte Chemie International Edition*, vol. 55, no. 21, pp. 6261-6265, 2016.
[63] H. Lorenz *et al.*, "Novel methanol steam reforming activity and selectivity of pure In2O3," *Applied Catalysis A: General*, vol. 347, no. 1, pp. 34-42, 2008.
[64] M. Dou, M. Zhang, Y. Chen, and Y. Yu, "Theoretical study of methanol synthesis from CO2 and CO hydrogenation on the surface of ZrO2 supported In2O3 catalyst," *Surface Science*, vol. 672, pp. 7-12, 2018.
[65] M. S. Frei *et al.*, "Mechanism and microkinetics of methanol synthesis via CO2 hydrogenation on indium oxide," *Journal of Catalysis*, vol. 361, pp. 313-321, 2018.
[66] T.-y. Chen *et al.*, "Unraveling Highly Tunable Selectivity in CO2 Hydrogenation over Bimetallic In-Zr Oxide Catalysts," *ACS Catalysis*, vol. 9, no. 9, pp. 8785-8797, 2019.
[67] C.-Y. Chou and R. F. Lobo, "Direct conversion of CO2 into methanol over promoted indium oxide-based catalysts," *Applied Catalysis A: General*, vol. 583, p. 117144, 2019.
[68] M. S. Frei *et al.*, "Role of Zirconia in Indium Oxide-Catalyzed CO2 Hydrogenation to Methanol," *ACS Catalysis*, vol. 10, no. 2, pp. 1133-1145, 2019.
[69] F. Chamssine, "Catalytic hydrogenation of CO2 to methanol over In-promoted Cu/ZnO/Al2O3 derived from hydrotalcite-like precursors," University of Stavanger, Norway, 2019.
[70] J. Gao, F. Song, Y. Li, W. Cheng, H. Yuan, and Q. Xu, "Cu2In nanoalloy enhanced performance of Cu/ZrO2 catalysts for the CO2 hydrogenation to methanol," *Industrial & Engineering Chemistry Research*, 2020.
[71] Z. Yu and K. Stangeland, "PET 635 Lecture 20: Methanol Synthesis and MTG," Universitetet i Stavanger, 2019.
[72] L. Gao, J. Li, and C. Au, "Mechanistic studies of CO and CO2 hydrogenation to methanol over a 50Cu/45Zn/5Al catalyst by in-situ FT-IR, chemical trapping and isotopelabelling methods," in *Studies in Surface Science and Catalysis*, vol. 130: Elsevier, 2000, pp. 3711-3716.
[73] L. Grabow and M. Mavrikakis, "ACS Catal. 2011, 1, 365," ed: DOI.
[74] Y.-F. Zhao, Y. Yang, C. Mims, C. H. Peden, J. Li, and D. Mei, "Insight into methanol synthesis from CO2 hydrogenation on Cu (1 1 1): complex reaction network and the effects of H2O," *Journal of Catalysis*, vol. 281, no. 2, pp. 199-211, 2011.
[75] J. Haber, J. Block, and B. Delmon, "Manual of methods and procedures for catalyst characterization (Technical Report)," *Pure and applied Chemistry*, vol. 67, no. 8-9, pp. 1257-1306, 1995.
[76] W. V. Knowles, M. O. Nutt, and M. S. Wong, "Supported metal oxides and the surface density metric," *Handbook of Catalyst Synthesis: The Science and Engineering of Catalyst Preparation*, pp. 251-281, 2007.
[77] G. Ertl, H. Knözinger, and J. Weitkamp, *Preparation of solid catalysts*. John Wiley & Sons, 2008.

[78] E. Marceau, X. Carrier, and M. Che, "Impregnation and drying," *Synthesis of Solid Catalysts*, pp. 59-82, 2009.
[79] F. Pinna, "Supported metal catalysts preparation," *Catalysis Today*, vol. 41, no. 1-3, pp. 129-137, 1998.
[80] S. Schimpf and M. Muhler, "Methanol catalysts," *Synthesis of Solid Catalysts*, pp. 329-351, 2009.
[81] M. Che and J. C. Védrine, *Characterization of solid materials and heterogeneous catalysts: From structure to surface reactivity*. John Wiley & Sons, 2012.
[82] H. L. Huynh, "Synthesis, characterization, and activity of bimetallic Ni-Fe hydrotalcite-derived catalysts in dry reforming of methane," University of Stavanger, Norway, 2018.
[83] S. Lowell, J. E. Shields, M. A. Thomas, and M. Thommes, *Characterization of porous solids and powders: surface area, pore size and density*. Springer Science & Business Media, 2012.
[84] G. Leofanti, M. Padovan, G. Tozzola, and B. Venturelli, "Surface area and pore texture of catalysts," *Catalysis today*, vol. 41, no. 1-3, pp. 207-219, 1998.
[85] O. Hinrichsen, T. Genger, and M. Muhler, "Chemisorption of N2O and H2 for the Surface Determination of Copper Catalysts," *Chemical Engineering & Technology: Industrial Chemistry-Plant Equipment-Process Engineering-Biotechnology,* vol. 23, no. 11, pp. 956-959, 2000.
[86] J. R. Jensen, T. Johannessen, and H. Livbjerg, "An improved N2O-method for measuring Cu-dispersion," *Applied Catalysis A: General*, vol. 266, no. 1, pp. 117-122, 2004.
[87] R. Thomas, *Practical guide to ICP-MS: a tutorial for beginners*. CRC press, 2013.
[88] H. Friedrich, P. E. de Jongh, A. J. Verkleij, and K. P. de Jong, "Electron tomography for heterogeneous catalysts and related nanostructured materials," *Chemical reviews*, vol. 109, no. 5, pp. 1613-1629, 2009.
[89] E. Lam, K. Larmier, S. Tada, P. Wolf, O. V. Safonova, and C. Copéret, "Zr (IV) surface sites determine CH3OH formation rate on Cu/ZrO2/SiO2-CO2 hydrogenation catalysts," *Chinese Journal of Catalysis*, vol. 40, no. 11, pp. 1741-1748, 2019.
[90] H. M. McNair, J. M. Miller, and N. H. Snow, *Basic gas chromatography*. John Wiley & Sons, 2019.
[91] F. G. Kitson, B. S. Larsen, and C. N. McEwen, *Gas chromatography and mass spectrometry: a practical guide*. Academic Press, 1996.
[92] O. D. Sparkman, Z. Penton, and F. G. Kitson, *Gas chromatography and mass spectrometry: a practical guide*. Academic press, 2011.
[93] C. Jeong and Y.-W. Suh, "Role of ZrO2 in Cu/ZnO/ZrO2 catalysts prepared from the precipitated Cu/Zn/Zr precursors," *Catalysis Today*, vol. 265, pp. 254-263, 2016.
[94] T. Witoon *et al.*, "Tuning of catalytic CO2 hydrogenation by changing composition of CuO–ZnO–ZrO2 catalysts," *Energy Conversion and Management*, vol. 118, pp. 21-31, 2016.
[95] X. Dong, F. Li, N. Zhao, F. Xiao, J. Wang, and Y. Tan, "CO2 hydrogenation to methanol over Cu/ZnO/ZrO2 catalysts prepared by precipitation-reduction method," *Applied Catalysis B: Environmental*, vol. 191, pp. 8-17, 2016.
[96] B. Liang *et al.*, "Investigation on deactivation of Cu/Zno/Al2O3 catalyst for CO2 hydrogenation to methanol," *Industrial & Engineering Chemistry Research*, vol. 58, no. 21, pp. 9030-9037, 2019.